

Department of Civil, Chemical, Environmental and Materials Engineering

MASTER'S DEGREE IN ENVIRONMENTAL ENGINEERING

Curriculum Climate Change Adaptation

DISSERTATION

in

Biotechnologies for the sustainable reclamation

of contaminated lands and waters M

**3D BIOPRINTING FOR SYNTROPHIC
BIOREMEDIATION OF TETRACHLOROETHYLENE**

Candidate

Federico Scutti

Supervisors

Prof. Fabio Fava

Prof. Philippe Corvini

Co-supervisors

Ana Dujmovic

Boris Kolvenbach

Academic Year 2021/2022

ABSTRACT	4
1. INTRODUCTION	5
1.1 POLLUTION BY POLYCHLORINATED HYDROCARBONS	5
1.2 WIDELY USED DECONTAMINATION TECHNOLOGIES	6
1.3 3D BIOPRINTING TECHNOLOGY AS A PERFORMANCE ENHANCER FOR BIOREMEDIATION	7
1.4 MATERIALS AND TECHNIQUES OPTIMISED FOR 3D BIOPRINTING AND BIOREMEDIATION	8
1.5 MICROBIAL ACTIVITY IN RELATION TO BIOREMEDIATION OF CHLORINATED HYDROCARBONS	8
1.6 3D BIOPRINTED SYSTEMS FOR BIOAUGMENTATION APPLICATION	9
2. OBJECTIVES AND CONSIDERATIONS	11
3. MATERIALS AND METHODS.....	12
3.1 CULTURE MEDIA PREPARATION	12
3.2 BACTERIAL CULTIVATION	12
3.3 SYNTHESIS OF METHACRYLATE MODIFIED SODIUM ALGINATE (MA-SA)	12
3.4 PHOTO-CROSSLINKERS PREPARATION.....	13
3.5 CROSSLINKING ASSAY.....	13
3.6 FOURIER TRANSFORM INFRARED SPECTROSCOPY ANALYSIS.....	13
3.7 PREPARATION OF HYDROGEL BIO-INK (BIOINK).....	14
3.8 USE OF 3D PRINTING IN BIOFILM PREPARATION	14
3.9 ANALYTICAL MEASUREMENTS WITH GC-FID SYSTEM	15
3.10 CONFOCAL MICROSCOPY	15
4. RESULTS.....	17
4.1 BACTERIAL GROWTH CURVE OF DSM14645 IN MEDIUM 1062	17
4.2 METHACRYLATED SODIUM ALGINATE (MASA) SYNTHESIS ANALYSIS BY DoE APPROACH	18
4.3 INFLUENCE OF MASA, CARRAGEENAN AND CARBOXYL-METHYL CELLULOSE ON BIOINK PROPERTIES	22
4.4 3D PRINTING DESIGN AND TECHNIQUES DEVELOPMENT	26
4.5 PCE DEGRADATION ASSAY	32
5. DISCUSSION.....	36
5.1 BACTERIAL GROWTH CURVE OF DSM14645 IN MEDIUM 1062	36
5.2 METHACRYLATED SODIUM ALGINATE SYNTHESIS ANALYSIS.....	36
5.3 3D BIOPRINTING	37
5.4 BACTERIAL SURVIVABILITY ASSAY IN 3D PRINTED OBJECTS	39
5.5 PCE DEGRADATION IN GROUNDWATER	41
6. CONCLUSION.....	44
7. ACKNOWLEDGEMENTS	46
8. BIBLIOGRAPHY	47
APPENDIX A – PROTOCOLS	53
APPENDIX B – IMAGES	57

Abstract

Perchloroethylene (PCE) is a common and persistent pollutant belonging to the family of dense non-aqueous phase liquids (DNAPL). This chlorinated hydrocarbon has properties that allow it to accumulate into the food chain, thereby harming both humans and the environment. One of the technologies adopted to remove such compound from contaminated sites is bioremediation, namely the exploitation of metabolic processes of plants and microorganisms for the degradation of contaminants to non-toxic by-products. This thesis focuses on the implementation of 3D printed systems with incorporated bacterial strains able to degrade PCE. The complete degradation of this pollutant is made possible by the syntrophic metabolism of two different strains of bacteria, namely the anaerobe *Desulfitobacterium hafniense* strain PCE-S, and the aerobe *Polaromonas* sp. strain JS666.

Optimisation of the protocols and stabilisation of the synthesis of methacrylated sodium alginate were the main focus of the project. The improved throughput and reliability obtained in the production of materials allowed to study the design of the bioink system, in order to identify appropriate shapes and printing conditions. The creation of a single-print, biocompatible object in which the two strains of bacteria were able to coexist could be achieved. These accomplishments represent the foundation for studies of PCE degradation potential of this system for its possible use in *in situ* bioremediation employments.

1. Introduction

1.1 Pollution by polychlorinated hydrocarbons

Environmental pollution is a widespread hazard that represents a major concern for many countries around the world, due to its numerous sources as well as potentially dangerous consequences. Among the most harmful types of pollutants are chlorinated hydrocarbons (CHCs), which form a big family of chemicals that includes organochlorine pesticides such as DDT, industrial chemicals such as polychlorinated biphenyls (PCBs), and chlorine waste products such as dioxins. These compounds are renowned for their high stability, that allows them to bioaccumulate in the environment and enter into the food chain (EEA, 2023). Chlorinated hydrocarbons are highly soluble in oils and fats, so they are able to accumulate in body tissues and therefore contribute in chronic toxicities (Bolla and Cadet, 2007; Malik et al., 2011). One such compound is tetrachloroethylene or perchloroethylene (PCE), a small, highly stable, hydrophobic and volatile molecule that has numerous uses in the industrial sector, from dry cleaning to metal degreasing (Cichocki et al., 2016; EPA, 2023; ECHA, 2023). PCE is a toxic chlorinated aliphatic hydrocarbon (CAH) that can pose major hazards to humans, primarily but not limited to cytotoxicity, acute encephalopathy and probable cause of cancer (Eicher, 2009; Cichocki et al., 2016; Kocaman and Asfuroğlu, 2021). Not only is PCE a persistent hazardous compound, but also its less chlorinated forms, naturally occurring from its anaerobic reductive dechlorination (ARD) pathway, are potentially dangerous toxicants (Cooper and Hanigan, 2010; Lyon and Vogel, 2011); these are trichloroethylene (TCE), *cis*-dichloroethylene (cDCE) and vinylchloride (VC), as shown in the pathway in Fig. 1.

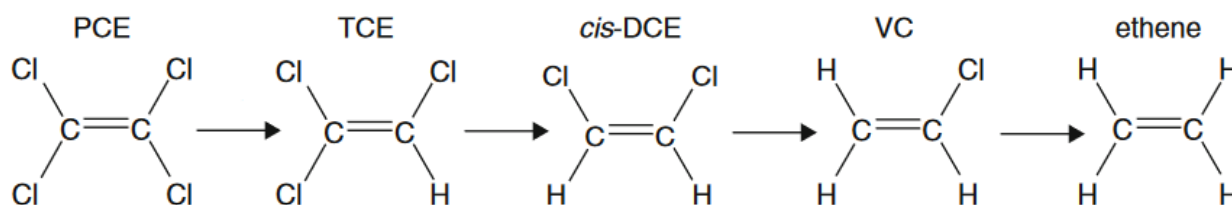


Fig. 1 – Reductive dechlorination pathway of PCE.

All of these halogens are pollutants commonly found in groundwater in the USA (Brusseau, 2019), further affirming their hazardous potential. TCE in particular is also widely used in the industry for metal degreasing, and contrary to PCE it's a known carcinogen (Cichocki et al., 2016).

Additionally, PCE and its intermediates are categorized as dense non-aqueous phase liquids (DNAPL). These are a class of pollutants that are particularly hard to handle, mainly because in porous media they are drawn in between solid grains in the unsaturated zone by capillary forces, where they form three-phase systems with air and water as shown in Fig. 2 (Sale and Newell, 2010). Thanks to gravity and capillary forces they are also able to migrate from sub-surface environments close to a source of contamination all the way to a nearby aquifer, where the soluble constituents of DNAPLs can slowly be partitioned into the groundwater (Rifai et al., 2010).

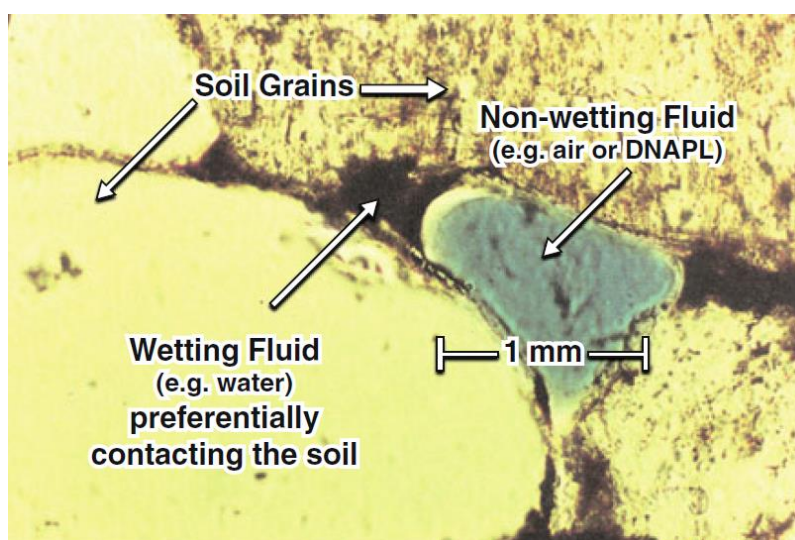


Fig. 2 – Immiscible fluid in the pore space of granular porous media.

Having low solubility in water, PCE and TCE are also likely to sink to the bottom of the aquifer, forming a pool from which they can be slowly released, polluting the site for a potentially very long period of time (Rifai et al., 2010).

1.2 Widely used decontamination technologies

Various approaches have been employed to decontaminate sites polluted by these chemicals, which can be categorized as in *in situ* or *ex situ*. Since for the scope of this thesis the focus will be on bioremediation, a remediation technique typically performed *in situ*, *ex situ* techniques will not be introduced or discussed. Therefore, it's worth mentioning some examples of *in situ* remediation techniques commonly used nowadays, such as soil vapor extraction, bioremediation and chemical oxidation (Kuppusamy et al., 2016).

All of these techniques require a thorough study of the hydrogeology and chemical properties of the site in which they are to be deployed, especially concerning chemical oxidation, where a selected chemical used as oxidant is injected into the soil to react with the pollutant. Common oxidants used in this approach are hydrogen peroxide and various persulfates and permanganates, which can be applied against many contaminants and in sites with different degrees of contamination, making chemical oxidation very flexible in these terms. On the other hand, the deployment of large quantities of chemicals in the environment with a specific purpose can lead to severe accidental consequences, if the aforementioned study of site characteristics is not performed properly. This can lead to the unintentional formation of other polluting by-products or a lower-than-expected removal of the main pollutants. For example, persulfates and hydrogen peroxide based oxidants like Fenton's reagent are able to generate non-selective free radicals that can react with a number of reduced compounds other than the target contaminants (McCarty, 2010).

Soil vapor extraction represents a cheaper solution compared to chemical oxidation, consisting simply in a system of vacuums and wells for the extraction of volatile organic compounds from the contaminated zone. Its relative simplicity makes it an approach that can be integrated with other techniques, such as bioventing, but also makes it susceptible to the volatility of the pollutants and to the geological properties of the soil. The success of this approach relies heavily on adequate air movements within the contaminated portion of the subsurface (Nobre and Nobre, 2004; Suthersan et al., 2016).

A third technology that can be applied to tackle an organochlorine contamination is bioremediation, which relies on microbes or plants to degrade or transform pollutants in contaminated environments. The organisms employed to do so can be naturally occurring or artificially introduced, enabling the

treatment of a wide variety of pollutants. A successful use of bioremediation techniques involves the transformation of said pollutants down to non-toxic end products such as water or carbon dioxide. Furthermore, bioremediation is a remarkably flexible technology (Brown, 2010), both in terms of environments in which it can be employed and pollutants that can be treated with it. More specifically, pollutants that cannot be completely converted to non-toxic products by a single microorganism are still degradable via consortial metabolism, also known as syntrophy, where the microbial community of a contaminated site evolves to allow the metabolism of the pollutants to be broken into many pathways, parts of which belong to a microorganism and parts to others (Suthersan et al., 2016).

It is important to note that syntrophic systems can consist of both aerobes and anaerobes bacteria simultaneously. The pathway shown in Fig. 1 is specific of ARD, but only some bacteria are capable of performing that entire dechlorination pathway. More specifically, some strains from the genus *Dehalococcoides* have the capability to transform PCE into ethene through ARD (Jugder et al., 2015), however *Dehalococcoides* are less robust than other halorespirers and the dechlorination rates of ARD decrease sharply as the number of chlorines decreases in CAH molecules (Chen et al., 2020; Xing et al., 2022). Alternatively to anaerobic processes, direct aerobic oxidation (DAO) is another dechlorination process in which a CAH such as cDCE, VC or even TCE, is metabolized by an aerobe as a source of carbon and energy (Xing et al., 2022). An aerobe performing DAO does not need additional supply of growth substrate, as the CAH will be his sole carbon source; oxygen-efficiency is very high thanks to the presence of very few oxygen-consuming reactions that are not associated to the CAH dechlorination. Finally, another advantage of DAO is that the CAHs are directly transformed into small molecule compounds, avoiding the formation of undesired and potentially toxic low chlorinated chemicals and degrading the pollutant thoroughly (Nijenhuis and Kuntze, 2016; Xing et al., 2022).

In the case of artificial bioremediation, consortial metabolism can be achieved by introducing the correct strain of bacterium (or multiple strains of bacteria, in case of syntrophy) to the contaminated matrix, in order for natural metabolization of chlorinated compounds to occur. Consequently, great significance resides in having an effective and efficient manner to deliver such bacteria to the target site.

1.3 3D bioprinting technology as a performance enhancer for bioremediation

3D printing technology has emerged as a promising approach for producing objects that can encapsulate target bacteria and enable their growth and transport for bioremediation scopes (Liu et al., 2022). This technology, referred to as 3D bioprinting, consists in extruding cell-laden biomaterial in a bottom-up, layer-by-layer approach until a previously designed three-dimensional (3D) construct is built (Campbell et al., 2019). With this approach it is possible to create complex structures that can host microbial growth while simultaneously being customizable to fit the specific needs of a given project (Correia Carreira et al., 2020). 3D bioprinting nowadays has uses in bioremediation, regenerative medicine and culture meat production. Furthermore, 3D bioprinting has great potential scalability, making it appealing for large-scale industrial bioprinting (Ramadan and Zourob, 2021). The choice of the material employed for 3D bioprinting is conditioned by the intended field of use. Widely used materials as bacterial carriers are hydrogels, which are highly hydrated polymeric networks used to homogeneously encapsulate cells and other biological molecules (Merceron and Murphy, 2015). The encapsulation of bacterial cells makes it possible to immobilize and transport them, allowing to potentially deliver them to target sites in the context of a bioremediation operation. For its use as a carrier for bioremediation, the hydrogel should be non-toxic for both hosted bacteria and the environment, water insoluble, inexpensive and stable. These properties can be obtained by choosing an appropriate molecule to create the hydrogel with, among the many organic and inorganic

substances available naturally or synthetically. Natural organic carriers are biodegradable and non-toxic compounds that fit well in a bioremediation context (Dzionic et al., 2016). An example of such compounds is alginate, a linear hydrophilic polysaccharide usually fitting for hosting cell-growth thanks to its characteristics of biocompatibility and porosity (Rastogi and Kandasubramanian, 2019; Drury and Mooney, 2003)

1.4 Materials and techniques optimised for 3D bioprinting and bioremediation

In order to improve the mechanical characteristics of hydrogels and materials used in 3D bioprinting technology, it is common practice to use crosslinking techniques to bond together chains of polymers to achieve decreased solubility or stiffness. Crosslinking is an irreversible chemical reaction that takes place between specific functional groups activated through the use of initiators (Rosato and Rosato, 2003). Such reaction can be obtained by irradiating the material with light at particular wavelengths in the presence of photo-initiators (Smeds and Grinstaff, 2001).

Alginate on his own is not able to photo-crosslink, so suitable functional groups need to be introduced chemically, such as methacrylate groups. The latter can be added to the alginate through the process of methacrylation. For example, methacrylation on sodium alginate with methacrylic anhydride yields methacrylated sodium alginate, which possesses methacrylic groups that can be photo-crosslinked in presence of initiators through exposure to green light (520 nm) (Charron et al., 2016).

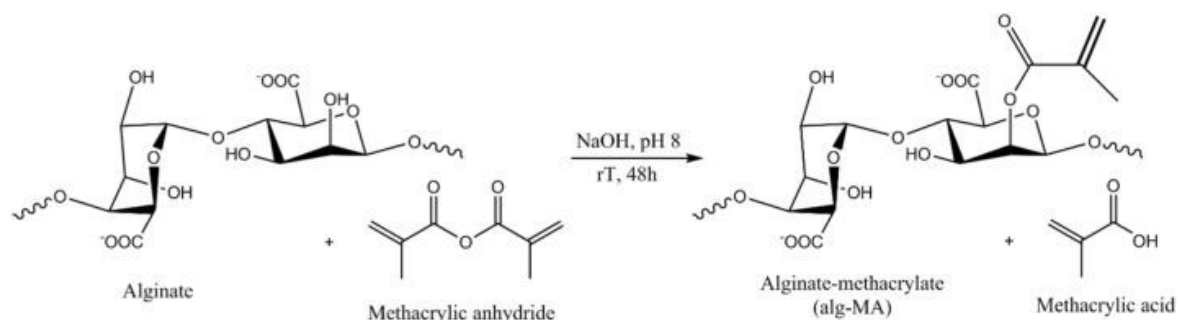


Fig. 3 – Methacrylation reaction on alginate, performed by reacting alginate with methacrylic anhydride yielding methacrylated alginate and excess methacrylic acid.

Methacrylated alginate is a promising material to use in hydrogel bioinks due to its excellent biocompatibility, tuneable mechanical properties, and ability to form stable hydrogels in the presence of divalent cations (Unagolla and Jayasuriya, 2020; Gao et al., 2022). However, the synthesis of methacrylated alginate can be challenging due to the high degree of substitution required for efficient crosslinking of the resulting hydrogels.

1.5 Microbial activity in relation to bioremediation of chlorinated hydrocarbons

As previously mentioned, bioremediation uses the metabolic activities of bacteria, fungi and plants to transform pollutants present in a contaminated site. For the scope of this thesis, we will focus only on microbial activities, in particular bacterial bioaugmentation for degrading CHCs.

Metabolic anaerobic reductive dechlorination is a biologically mediated reaction where microorganisms gain energy as one or more chlorine atoms are replaced with a hydrogen in an anaerobic environment. The electron acceptor in such reaction is the CHC, while typically molecular hydrogen works as the electron donor, supplied through the fermentation of organic substrates (Henry, 2010). If the metabolic activity of the bacteria present in a contaminated site is known to degrade pollutants such as chlorinated solvents down to a harmless chemical like water or ethene, bioremediation can be effectively performed on that site by delivering a fermentable organic

substrate or a direct electron donor in a process called biostimulation. This makes it so that microbial growth is stimulated by the enhanced electron donor availability, promoting anaerobic degradation of the chlorinated solvents that are used as electron acceptors (Henry, 2010). Even though biostimulation has been applied successfully in hundreds of sites (Leeson et al., 2004) and microbial populations able to anaerobically degrade highly chlorinated compounds can be found in almost any subsurface environment (Henry, 2010), there are obstacles in using this technique that can limit or even preclude its use. For example, the anaerobic dechlorination of PCE and TCE to cDCE is performed by halorespiring bacteria in most sites around the globe, but, as mentioned above, for energetic and kinetic constraints the dechlorination process does not progress to VC and ethene (Bradley and Chapelle, 2010; Henry, 2010). The risk of accumulation of volatile or toxic by-products therefore would be enhanced by the use of biostimulation.

In sites where the native microbial community is not able to achieve complete anaerobic reductive dechlorination of chlorinated solvents, specific bacterial population may need to be added to effectively perform the required transformation. Counterposed to biostimulation, this process takes the name of bioaugmentation, a different technique for boosting biological activity that improves the rate and extent of reductive dechlorination (Lendvay et al., 2003). Bioaugmentation can be used in alternative to biostimulation if the native microbial population is unable to perform the appropriate transformation to the target pollutant, but can also enhance its degradation performance by reducing the time that these bacteria need to acclimate and grow under the new conditions of added substrate, or by working as a contingency measure in case the biostimulation process stalls at a particular intermediate by-product. Like any other bioremediation technique, bioaugmentation performance on a contaminated site is influenced by many factors: exposure to oxygen, competition for electron donor, type and concentration of electron donor used, temperature, pH, concentrations of the target chlorinated solvents and the presence of other chlorinated solvents. Therefore, a period of preconditioning of a target contaminated aquifer is often necessary in order to establish the desired oxidation-reduction potential (ORP) before performing bioaugmentation (Ellis et al., 2000; Major et al., 2002; Stroo et al., 2010).

1.6 3D bioprinted systems for bioaugmentation application

Based on the findings what stated so far about the use of innovative techniques for the bioremediation of sites polluted by PCE and its metabolites, this thesis aims at developing of a system that leverages all the technologies mentioned above for the remediation of contaminated sites. Such system would host two different strains of bacteria that coexist and grow in a hydrogel bioink matrix, one aerobe and the other anaerobe. In presence of the appropriate biogeochemical conditions, aerobic and anaerobic bacteria can thrive side by side within biofilms while also collaborating to share metabolic by-products (Suthersan et al., 2016). The goal is to have this system syntrophically degrade chlorinated solvents such as PCE, TCE, cDCE and VC, reducing them down to innocuous ethene.

The bacterial strains employed in this project are *Desulfitobacterium hafniense* strain PCE-S (further referred to as DSM14645, its strain name in the German Collection of Microorganisms and Cell Cultures database from the Leibniz Institute) and *Polaromonas* sp. strain JS666 (JS666), available in the American Type Culture Collection under strain name BAA-500. DSM14645 is an anaerobic bacteria known to be capable of reductive dechlorination (Christiansen and Ahring, 1996). In particular, it is able to degrade PCE and TCE (Holliger et al., 1998; Jugder et al., 2015), using these molecules as the electron acceptor in the metabolic reduction processes described in section **1.5 Microbial activity in relation to bioremediation of chlorinated hydrocarbons**. On the other hand, JS666 is an aerobe capable of completing the dechlorination of cDCE and VC through DAO (Xing et al., 2022).

These bacteria are to be fixed in a 3D bioprinted structure that should provide a non-toxic growth environment for both strains. The design of these structures is supposed to perform in an array of contexts, not only in terms of nutrients and oxygen concentrations but also in terms of transport and deployment in a bioremediation setting. Although 3D bioprinting represents a promising technology for the development of complex multi-functional biological systems, reliability and reproducibility of these methods have so far been challenging (Ke et al., 2021).

2. Objectives and considerations

The research focuses on the synthesis of the hydrogel bioink and its components, as well as on the bioremediation process itself. More specifically, great importance is given to methacrylated sodium alginate (MASA), as the main component of the hydrogel bioink, and its synthesis process. To overcome this, improvements are made to the MASA synthesis process, as well as studies on different 3D bioprintable designs, in order to allow for the stable and efficient production of these hydrogel bioink-based systems. Moreover, the research focuses on optimizing these procedures to improve the mechanical properties of the resulting hydrogels and to ensure the viability and functionality of the encapsulated bacteria. Further experiments are conducted on PCE depletion performance of said systems, although these can be considered only preliminary and not definitive.

3. Materials and methods

The exact protocols that have been followed and that are described in the following can be found in **Appendix A**.

3.1 Culture media preparation

Medium 1062 for the cultivation of *Desulfitobacterium hafniense* strain PCE-S (DSM 14645) has been prepared according to a revised version of DSMZ official medium recipe #S2152 (Main sol. 1062) (Koblitz et al., 2023).

Tryptic soy broth ¼ strength culture medium (TSB ¼) has been prepared according to ATCC medium #2329 (Rédei, 2008) for strain JS666.

3.2 Bacterial cultivation

The original culture of *Desulfitobacterium hafniense* strain DSM14645 has been purchased from “*Deutsche Sammlung von Mikroorganismen und Zellkulturen*” (DSMZ) as an actively growing culture. This has been inoculated 200 µl into 50ml freshly prepared Medium 1062 for sub-cultivation, incubating at 30 °C, in non-shaking incubator (model Heraeus™ Kendro). Same conditions have been applied to following sub-cultures. Growth has been monitored using a SynergyH1 microplate reader from BioTek™. The growth curve has been traced with values of optical density at a wavelength of 600nm (OD₆₀₀). OD₆₀₀ is a measure of the concentration of cells in a liquid, commonly used to indicate the growth stage of cultured cell population, for instance whether it is in the lag phase, log phase, or stationary phase (Sutton, 2006).

The original culture of *Polaromonas* sp. JS666 (ATCC® BAA-500™) has been purchased from the “*American Type Culture Collection*” (ATCC). Sub-culturing has been carried by preparing 0.5% cultures in 40ml of TSB ¼ within Erlenmeyer flasks, incubating in a thermoshaker IKA™ ks 4000 at 25 °C, 110 rpm. Growth has been monitored as described previously by measuring OD₆₀₀.

All of the biological lab work has been done in a Kojair™ biosafety class 2 BioWizard Silver Line biosafety cabinet.

To have a promptly access to active cultures of JS666, cryostocks have been prepared using 40% glycerol solution at -80 °C. Same incubation conditions as previously mentioned have been applied to sub-cultures deriving from defrosted cryostocks.

3.3 Synthesis of methacrylate modified sodium alginate (MA-SA)

The methacrylated sodium alginate (MA-SA) has been prepared by reacting a 2 % [w/V] aqueous solution of sodium alginate (SA) with a 20-fold [V/w] excess of methacrylic anhydride (MA) under rough stirring at 5° C for 48 h. The MA has been added to the sodium alginate solution under a chemical safety hood with the SA solution kept cool in an ice bath. Before the start of the reaction time of 48 h, an additional 22 – 25 ml of sodium hydroxide (NaOH) 5M has been added for every 100 ml of SA in order to increase pH to 8. The NaOH has been added dropwise over a period of about 30 minutes, while still keeping the solution in ice under rough stirring. To remove remaining methacrylic acid, methacrylic anhydride and other impurities, the modified suspension has been precipitated and washed with absolute ethanol 1:1 volume for at least four times, with centrifugation steps between each washing at 4'500 x g for 10 min at 4° C. The centrifuge used was an Eppendorf™ 5804 R. The sample has been dried overnight at room temperature (RT) under chemical safety hood to remove residual ethanol.

Before being considered ready to use, freshly prepared MA-SA was tested by photo-crosslinking assay and Fourier Transform Infrared Spectroscopy (FTIR) analysis. Further discussion of these two assessments can be found in the following paragraphs.

3.4 Photo-crosslinkers preparation

The agents used in the photo-crosslinking process have been prepared by creating a solution of 0.5% Eosin Y (EY) in 1-Vinyl-2-pyrrolidinon (VP) mixed with 5M triethanolamine (TEA) in 0.1M HEPES buffer stock solution at pH 7.4.

The final photo-crosslinking solution volume depends on the volume of bioink that needs to be photo-crosslinked. Per millilitre of bioink, 55 μ l of solution has been added with the following composition:

- 5 μ l of 0.5% EY in VP
- 50 μ l of 5M TEA in 0.1 HEPES buffer (pH 7.4).

Preparation has been carried out in presence of minimal light to avoid unwanted premature photo-crosslinking.

3.5 Crosslinking assay

The ability of freshly prepared MA-SA stocks to photo-crosslink has been tested upon preparation by performing a crosslinking assay. For the assay, 2 ml of aqueous solution of 2% [w/V] MA-SA solution has been prepared for each separate MA-SA stock (in a 6-well plate) and 110 μ l of photo-crosslinker solution added, namely 0.5% Eosin Y (EY) in 1-Vinyl-2-pyrrolidinon (VP) mixed with 5M triethanolamine (TEA) in 0.1M HEPES buffer stock solution at pH 7.4. Each sample has been mixed until homogeneous and photo-crosslinked by exposure to green light for up to 30 minutes. After photo-crosslinking, the container of choice in which the assay took place has been tilted to about 45° and the behaviour of the samples observed. The MA-SA used in the less fluid sample has been considered more reliable. This is because the inability to photo-crosslink suggests the persistence of MA groups in the final product due to improper washing, from which comes the stifling of photo-crosslinking.

3.6 Fourier Transform Infrared spectroscopy analysis

Fourier Transform Infrared Spectroscopy (FTIR) has been used to analyse the chemical composition of freshly prepared MA-SA, more specifically to look for potential impurities or faults from the preparation process.

After overnight drying, a sample of freshly prepared MA-SA has been analysed in an Agilent's Cary 630 FTIR Spectrometer. The dried MA-SA has been carefully placed and secured under the Diamond-ATR module of the machine, which has been previously cleaned with acetone. Data was acquired with Agilent's software MicroLab. FTIR output values have then been normalized to the strongest peak (lowest transmittance) in the wavelength region of methyl group around value of 2960 cm^{-1} (Bradley, 2015). These values have been used to draw transmittance [%] over wavelength [cm^{-1}] curves, whose peaks correspond to the presence of predetermined types of bonds, with which purity of MA-SA could be evaluated.

3.7 Preparation of hydrogel bio-ink (bioink)

For the preparation of abiotic bio-ink, synthesized and dried MA-SA has been rehydrated to a 2% [w/V] solution in water, heated to 80° C to dissolve completely under continuous rough stirring for at least 2 hours. Subsequently, ι -Carrageenan (CA) and Carboxymethyl cellulose (CMC) have been added respectively in 1.3% [w/V] and in 1.5% [w/V] under rough stirring, to be used as stabilizing agents. In between the additions, the solution was continuously heated until complete dissolution (about 2 hours each time) to obtain a homogeneous transparent liquid.

For biotic bio-ink, a similar procedure has been followed; water has been substituted with the medium used for the cultivation of the specific strain intended for that batch of ink: TSB ¼ has been used when preparing aerobic bioink to be inoculated with JS666 and Medium 1062 has been used when preparing anaerobic bioink to be inoculated with DSM14645. After having dissolved the powders and having obtained a homogeneous gel, a certain amount of defined bacterial culture growing at end of mid-exponential phase has been inoculated into the freshly prepared bioink under sterile conditions in order to reach a desired theoretical OD₆₀₀ of 0.5. When needed, bacterial cultures have been centrifuged at 4'500 x g for 10 minutes and the pellet re-suspend in low volume to significantly increase the concentration of cells in the inoculum for the bioink.

Anaerobic bio-ink has been prepared under constant anoxic conditions: the media has been transferred into the glove box in a sealed serum bottle and the powders and the MA-SA have been carried in Eppendorf vials or Falcon tubes. The glove box used was a custom-built GS™ glovebox equipped with an Eppendorf™ 5424 R centrifuge and an IKA™ RET Basic magnetic stirrer with heating plate.

Finally, photo-crosslinkers have been added in the previously mentioned concentrations (5µl of 0.5% EY in VP and 50µl of 5M TEA in 0.1 HEPES buffer pH 7.4 per ml of bioink prepared) immediately before printing to minimize exposure to visible light and therefore avoid premature crosslinking.

3.8 Use of 3D printing in biofilm preparation

For 3D printing of microbial biofilms, a 3DDiscovery™ Evolution Bio-printer (RegenHU, Fribourg; CH) has been used, consisting of four different printheads (PHs). For the design of the 3D object, the software from regenHU BioCad has been used. Furthermore, the 3D CAD model has been translated with the Slic3r software into coordinates and instructions (G-Code) for the 3DDiscovery™, allowing the bio-printer to move according to the defined path. Before starting the printing process, the axes of the printer have to be calibrated as described in the manufacturer's manual. It is also possible to use two PHs for the printing of 3D structures. A Computer Aided Design (CAD) file has been produced and transformed into a three-dimensional solid structure using an extrusion-based 3D-bioprinting technique with X, Y and Z stage controls. Extrusion pressure-based (pressure: 70 – 100 kPa, feed rate: 15 – 35 mm/s, layer thickness: 150 – 350 µm) and mechanically driven (flow rate: 10 – 30 µL/s, feed rate: 20 – 40 mm/s, layer thickness: 200 – 400 µm) printheads have been used for the printing process during trials. The parameters have been adjusted dynamically with the intent of finding a set of values that would be reliable regardless of the prepared bioink's properties. The final settings that have been employed for the printing method were:

- Mechanically driven extrusion with 2.5 ml Gastight Syringe 1005 TLL, PTFE Luer Lock and 5.0 ml Gastight Syringe 1005 TLL, PTFE Luer Lock from Hamilton and a stainless steel Luer Lock tapered tip from RegenHU with internal diameter 0.2 mm
- Feed rate: 15, layer thickness: 0.2 mm, no laser, no pressure, no cleaning, 0 strand start delay for the 2.5 ml syringe
- Feed rate: 30, layer thickness: 0.2 mm, no laser, no pressure, no cleaning, 0 strand start delay for the 5.0 ml syringe

The cells have been printed within hydrogel-based bio-ink matrix and the printed object photo-crosslinked by exposure to green light (approximately 520 nm) for 1-3 minutes in case of water-based bioink and 5-10 minutes in case of media-based bioink.

This setup has been employed to find the optimal design to be used in the PCE degradation assay.

3.9 Analytical measurements with GC-FID system

Chlorinated aliphatic hydrocarbon (CAH) tetrachloroethene (PCE) and its pathway intermediates in both simulated groundwater and culture media matrix have been measured by gas chromatography with flame ionization detector (GC-FID). Using a 10 μ l syringe (Hamilton, model 1701 N), 200 nl pure PCE have been spiked into headspace screwcap vials containing 7 ml of groundwater or TSB media with the following setup:

- 3x abiotic bioink print soaked into 7 ml of sterile groundwater
- 3x biotic bioink print inoculated with both JS666 and DSM14645 soaked into 7 ml of groundwater
- 3x 718 μ l inoculum of JS666 in groundwater
- 3x 200 μ l inoculum of DSM14645 in groundwater
- 3x 718 μ l inoculum of JS666 and 200 μ l inoculum of DSM14645 in groundwater
- 3x 718 μ l inoculum of JS666 and 200 μ l inoculum of DSM14645 in TSB media

The groundwater has been replicated by using mineral water with the composition listed in Table 1.

Compound	[mg/l]	Compound	[mg/l]
Ca ²⁺	80	Cl ⁻	10
Mg ²⁺	26	NO ₃ ⁻	1
Na ⁺	6.5	SiO ₂	15
K ⁺	1	F ⁻	0.1
HCO ₃ ⁻	360	Pb ²⁺	0
SO ₄ ²⁻	14	Cu ²⁺ / Zn ²⁺	0

Table 1 - Mineral composition of simulated groundwater stock used in setup for PCE degradation assay.

The volume of the inoculum has been decided after estimating the theoretical OD₆₀₀ of the inoculated prints, in order to have the same number of cells of each strain of bacteria in every vial with a non-abiotic content. In our setup, target theoretical OD₆₀₀ of inoculated prints was 0.7 for both bacteria, with a volume of 1.2 ml for the aerobic bioink and a volume of 0.1 ml for the anaerobic bioink.

The vials were filled in sterile conditions and immediately sealed with Teflon-coated caps. 250 μ l samples for gas chromatography have been withdrawn from the vials' headspace with a 250 μ l syringe (Hamilton, model 1725 SL) after flushing the syringe twice and manually injected into the GC-FID.

The system used was the following:

- Gas chromatographer with flame ionization detector (GC-FID) from Agilent Technologies model 7890A with inlet-split ratio 10:1 (45.48 ml/min total)
- Temperature: FID (300 °C), multi-mode inlet (280 °C), oven (40 °C to 190 °C, gradient: 20 °C/min)
- Flow: H₂ (30 ml/min), air (400 ml/min)
- Column: DB-624 125-1334 [30 m (L) x 0.53 μ m (I.D.) x 3 μ m (film)]; Front inlet to FID; SN# US1559087H

Note: MS was not used in this system.

3.10 Confocal microscopy

With the help of fellow scientist Dr. Joachim Köser, research associate at FHNW Institute for Chemistry and Bioanalytics and specialist in operating the laser scanning confocal microscope present at the facility, it was possible to look into biotic hydrogel samples using confocal microscopy.

The samples, consisting of 0.2 ml of anaerobically inoculated bioink, have been prepared by performing a live/dead cell staining with 1 μ l of 0.1 mM SYBR Green for living cells and 0.1 mM propidium iodide for dead cells. Stains have been mixed to the bioink manually with a spatula inside a 96-well plate. All of the above (anaerobic hydrogel preparation and inoculum plus cell staining) was performed in a glovebox in anoxic conditions; before taking out the well plate, the wells were sealed with gas-impermeable sealing film. After an incubation of 45 minutes to let the stains permeate through the cells walls, the samples were brought to the microscope. Here, Dr. Köser set up the well plate for the observation, removing the sealing film and turning on the N₂ flow in the chamber that hosted the samples. This flow was supposed to provide close to anoxic conditions. Other microscope parameters and settings employed to perform the observation had been set by Dr. Köser and are out of the scope of the thesis, therefore they will not be included.

4. Results

4.1 Bacterial growth curve of DSM14645 in Medium 1062

Growth curves of DSM14645 in Medium 1062 are shown in Fig. 4, displaying their growth over the span of 69 hours. The cultures were inoculated with a 7 hour gap from each other. The delay in inoculation was meant to fill the timepoint gaps between $t = 12$ and $t = 24$ and between $t = 34$ and $t = 49$, but unfortunately the growth of the second triplet started with a 7 – 8 hours delay as well, invalidating the attempt.

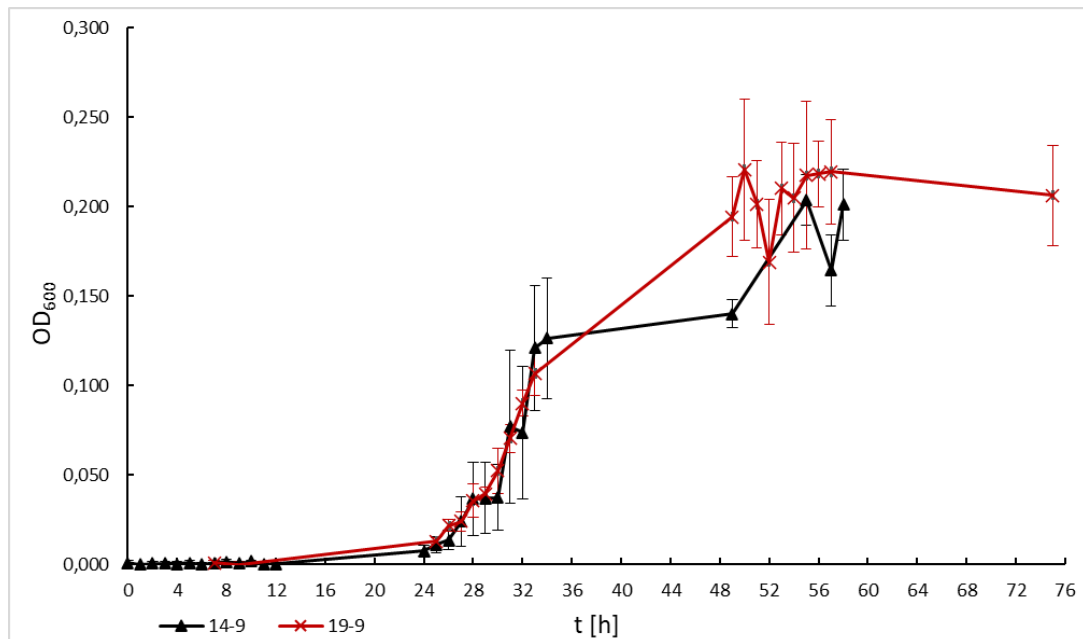


Fig. 4 – Collected timepoints of *Desulfitobacterium hafniense* strain DSM14645 growth in Medium 1062. First triplet of cultures (black) was inoculated on September 14th at 7:20 and second triplet (red) was inoculated on September 19th at 15:00.

To obtain a full growth curve the datapoints were then interpolated with a logistic regression using the Matlab programming language:

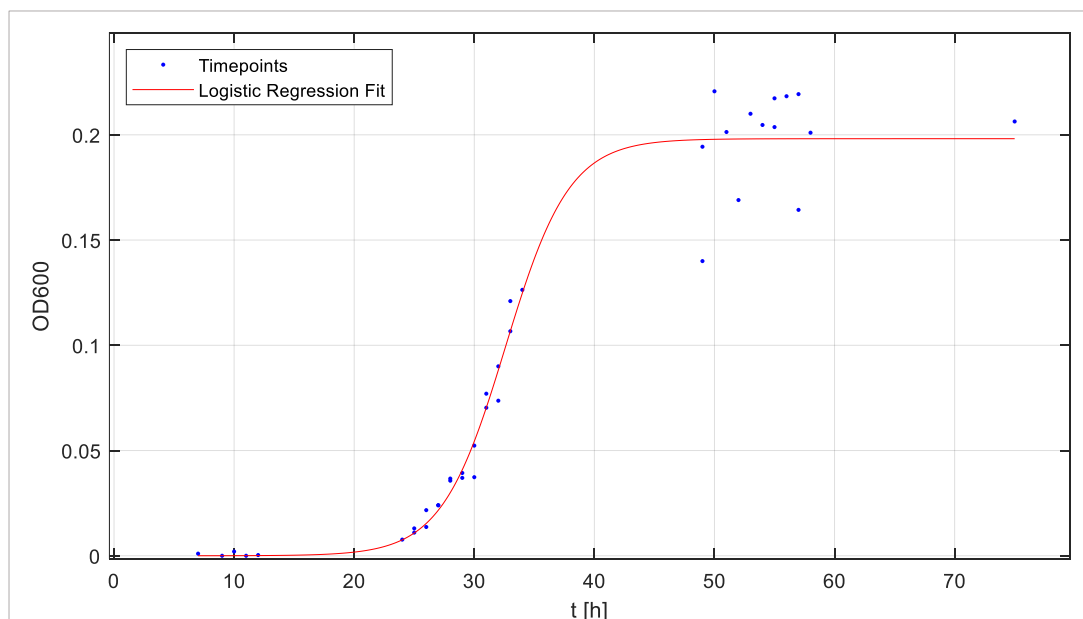


Fig. 5 – Growth curve of *Desulfitobacterium hafniense* strain DSM14645 in Medium 1062 as a logistic regression curve fitted to empirically measured timepoints

4.2 Methacrylated sodium alginate (MASA) synthesis analysis by DoE approach

The conditions in which MASA synthesis reaction takes place have been investigated in order to address the influence that each of them has on the final product. The approach used was that of a Design of Experiment (DOE) with the focus on the ability of the final product to yield homogeneous and photo-crosslinking hydrogel. The statistical software used to set the DOE was STAVEX, which was fed the following parameters:

- Response variables:
 - Crosslinking ability: [0:1]
 - FTIR cleanness: [0:1]
 - Yield: [0:100]%
- Factors:
 - MA overshoot: 1x, 2x, 4x, 8x, 16x, 32x
 - NaOH addition time: 0, 15, 30 min
 - Total reaction time: 24, 48, 72 h

Relevant interactions were set only between the MA overshoot and the reaction time. The highest scoring design was a Box-Behnken Optimisation over the following 13 different reaction conditions:

Run	MA overshoot [x]	NaOH add. speed [min]	Reaction time [h]	SA [g]	dH ₂ O [ml]	MA [ml]	NaOH [ml]	tot V [ml]	NaOH / min [μl]	NaOH add start [μl]	plate, well
1	4	0	24	0.11	5.5	0.44	1.265	7.21	0	1265	1b.1
2	4	30	24	0.11	5.5	0.44	1.265	7.21	42	5	1b.2
3	1	15	24	0.11	5.5	0.11	1.265	6.88	84	5	1b.4
4	32	15	24	0.11	5.5	3.52	1.265	10.29	84	5	1b.5
5	4	0	72	0.11	5.5	0.44	1.265	7.21	0	1265	3.1
6	4	30	72	0.11	5.5	0.44	1.265	7.21	42	5	3.2
7	1	15	72	0.11	5.5	0.11	1.265	6.88	84	5	3.4
8	32	15	72	0.11	5.5	3.52	1.265	10.29	84	5	3.5
9	32	0	48	0.11	5.5	3.52	1.265	10.29	0	1265	2.1
10	32	30	48	0.11	5.5	3.52	1.265	10.29	42	5	2.2
11	4	15	48	0.11	5.5	0.44	1.265	7.21	84	5	2.3
12	1	0	48	0.11	5.5	0.11	1.265	6.88	0	1265	2.4
13	1	30	48	0.11	5.5	0.11	1.265	6.88	42	5	2.5
14	32	30	72	1	50	32	11.5	93.5	383	10	4.4
15	32	0	24	1	50	32	11.5	93.5	0	11500	4.5

Table 2 – Overview of reaction parameters for optimisation of MASA synthesis conditions. Run 14 and 15 correspond to the confirmatory runs.

The different batches were prepared following the protocol previously shown in section 3.3 **Synthesis of methacrylate modified sodium alginate (MA-SA)** with the addition of a photo-crosslinking assay and a FTIR analysis on the yielded product after point 6 (FTIR analysis and photo-crosslinking assay have their own protocols, that can be found in section 3.5 **Crosslinking assay** and 3.6 **Fourier Transform Infrared spectroscopy analysis** respectively).

The yielded products' characteristics were summarized in the following table:

Run	pH SA	pH SA+ MA	pH + NaOH	T add. end [°C]	visual description	yield [%]	cross-linking	rep: cross-linking	Remarks
1	8	5	14	11	beige crumbs	79	0.1	0.1	insoluble at 80°C
2	8	6	14	12	beige crumbs + white flakes	84	0.1	0.1	insoluble at 80°C
					white flakes				
3	8	6	14	12	beige crumbs + yellow beads	96	0	0.1	
4	8	4	11	12	white flakes	168	0	0	insoluble at 80°C
					partially transparent, milky white crumbs	212	0	0	insoluble at 80°C
					completely transparent puddle	628	0	0	insoluble at 80°C
5	8	6	13	9	beige crumbs	83	0	0.1	
6	8	6	13	12	beige crumbs	82	0	0.1	
7	8	7	14	12	yellow beads	85	0.1	0	
8	8	5	6-10	12	white flakes	68	0.1	0.7	inhomogeneous upon NaOH addition
					partially transparent, milky white crumbs	465	0	0	insoluble at 80°C, inhomogeneous upon NaOH addition
9	8	4	6-12	9	white flakes	282	0	0	insoluble at 80°C, inhomogeneous upon NaOH addition
					partially transparent, milky white crumbs	427	0	0	insoluble at 80°C, inhomogeneous upon NaOH addition
					completely transparent puddle	422	0	0	insoluble at 80°C, inhomogeneous upon NaOH addition
10	8	4	10+	12	white flakes	54	0	0.7	insoluble at 80°C, inhomogeneous upon NaOH addition
					partially transparent, milky white crumbs	185	0	0	insoluble at 80°C, inhomogeneous upon NaOH addition
					completely transparent puddle	817	0	0	insoluble at 80°C, inhomogeneous upon NaOH addition
11	8	5	12.5	12	beige crumbs	96	0.1	0.1	
12	8	6	14	9	yellow beads	85	0	0	
13	8	6	14	12	yellow beads	93	0	0	
14	8	5	9-12	-	white crumbs + beige crumbs	70		1	inhomogeneous upon NaOH addition
15	8	5	10+	-	white crumbs	66		0.9	inhomogeneous upon NaOH addition

Table 3 – Overview of yielded products form optimisation of MASA synthesis conditions. The different pH stages correspond to SA only, after addition of MA and after complete addition of NaOH, followed by the Temperature readout at the timepoint of finished NaOH addition.

Changing MA concentrations in the reaction resulted in the most visible effect on the product appearance. These changes were especially evident on the colour, which ranged from yellow, compared to previously observed brown to white, to completely transparent gelatinous formations as the ratio of MA to SA increased. As this evidence would have suggested, MA overshoot was found by STAVEX to be the factor with the higher impact across all response variables, as can be seen in Fig. 6 in relation to photo-crosslinking ability.

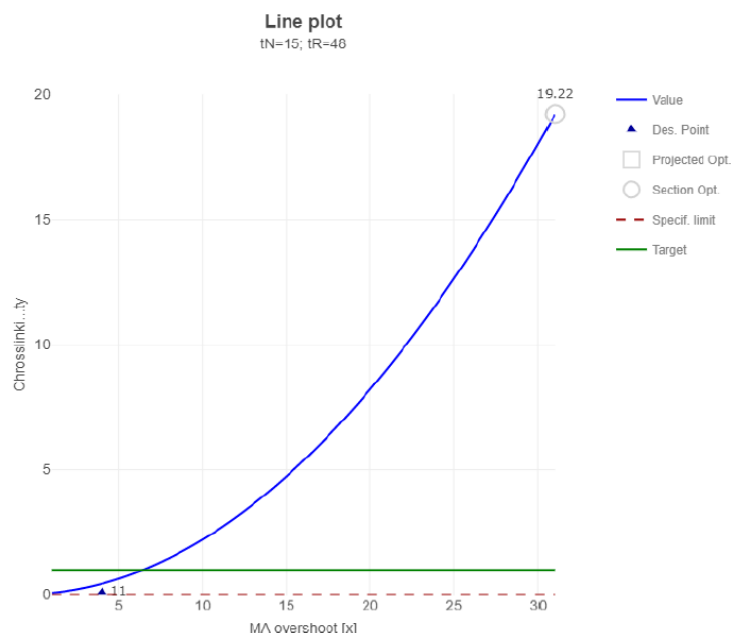


Fig. 6 – Plotted values of response variable Crosslinking ability over values of impact factor MA overshoot from fitted model (least-squares) with the highest R^2 value.

FTIR analysis was performed also on the single components (pure MA and pure SA) and a batch of MASA which was known to give good crosslinking results. Data from the experiment was normalized to the strongest peak (lowest transmittance) in the wavelength region of methyl group around value of 2960 cm^{-1} .

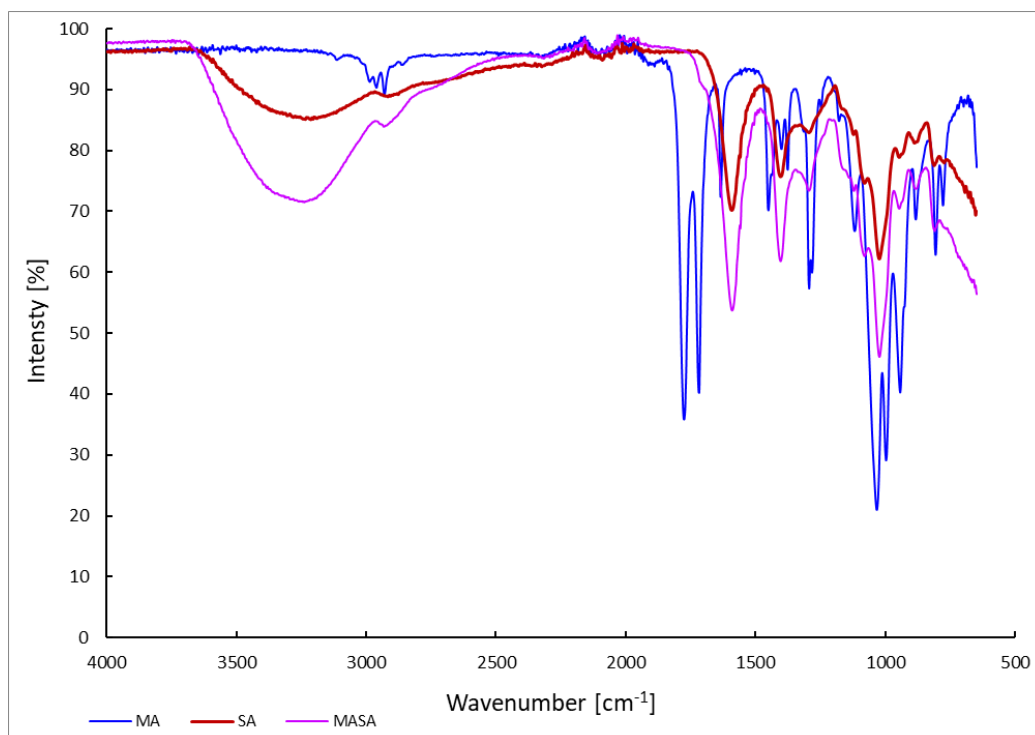


Fig. 7 – FTIR spectrum of starting materials and a previous crosslinkable MASA stock used as reference.

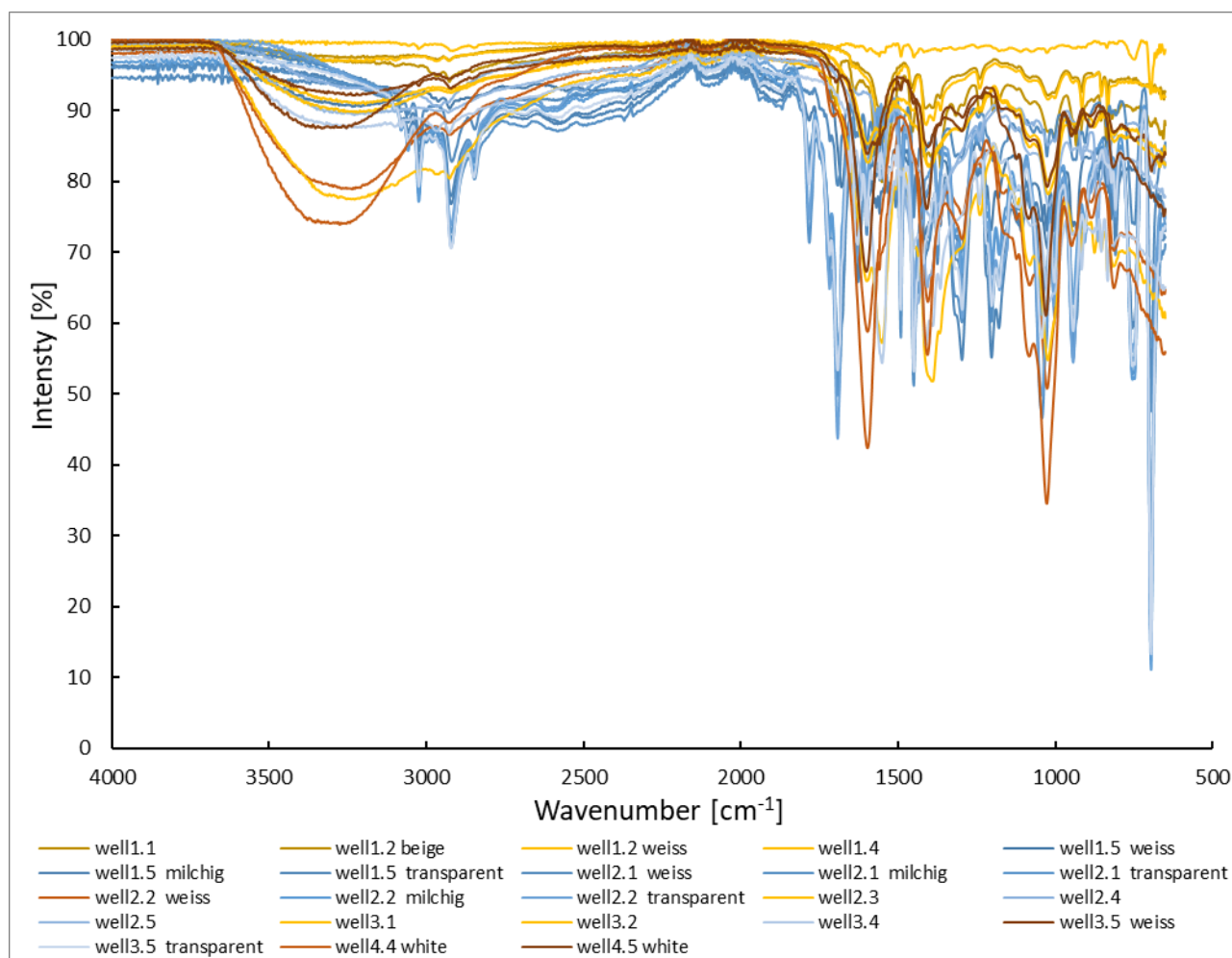


Fig. 8 – FTIR spectra of all yielded samples of the MASA synthesis optimisation reactions, color-coded by manually correlating the single curves of the samples to their ability to photo-crosslink (photo-crosslinking assay), with blue representing samples with no observable photo-crosslinking at all, yellow curves representing samples with increased viscosity after exposition to green light and red curves representing samples able to solidify upon exposition to green light.

Key differences in the positions of the peaks can be noticed easily, namely the very wide acid's OH-bond curve between 3000 and 3500 cm^{-1} present in SA and MASA and the cluster of strong peaks around 3000 cm^{-1} , which is present only in MA.

Moreover, curves were examined in the fingerprint region of the graph (between 500 and 1000 cm^{-1}). A clear distinction between the crosslinking and non-crosslinking sample groups can be seen by plotting the slope of the intensities in the wavelength range 650 – 800 cm^{-1} , as seen in Fig. 9, where the slope of blue curves (non-crosslinking) reaches lower in the negative values compared to yellow and red curves. In this figure, the curve of pure MA was overlaid as reference (dark blue) along with pure SA (dark red) and a previously well synthesised MASA (magenta).

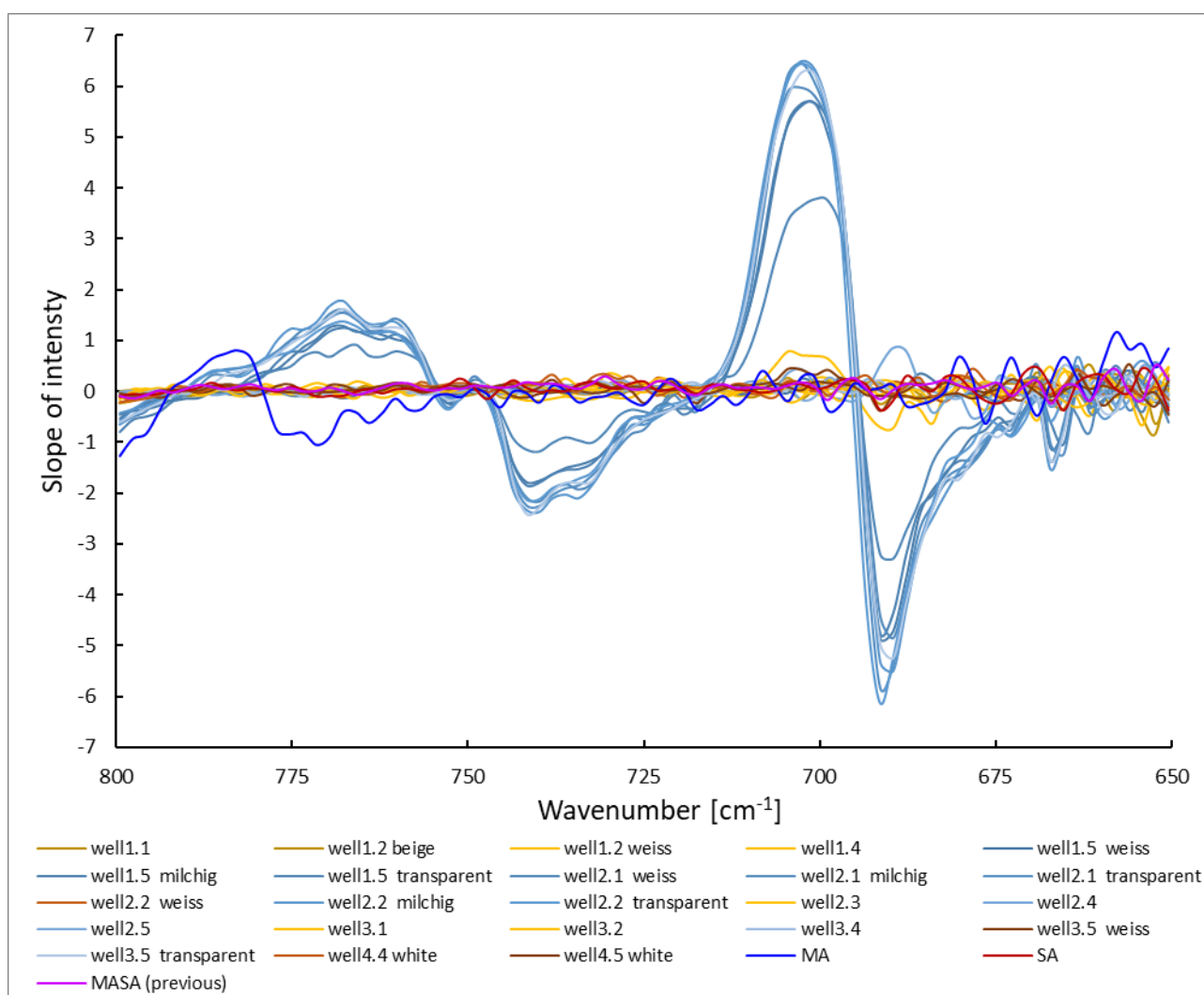


Fig. 9 - Slope of FTIR Intensities for fingerprint region of all yielded samples of the MASA synthesis optimisation reactions (blue: non-crosslinking, yellow: increasing viscosity, red: photo-crosslinking) overlaid with slope of intensities for the reference curves of MA in dark blue, SA in dark red and MASA in magenta.

By adding the reference curves of pure MA, pure SA and the previous stock of MASA, a clear distinction of the dark blue MA from the red positive curves can be noticed, but to the opposite of the blue negative group and flattening out very fast, while the negative group keeps oscillating.

4.3 Influence of MASA, Carrageenan and Carboxyl-methyl cellulose on bioink properties

During periods of frequent printing activities, it was necessary to prepare batches of bioink multiple times per week. Storing gel for more than a few days was avoided if possible as it greatly increased the risk of contamination and/or drying out, increasing its viscosity and hindering the printing process. In order to consistently have ready-to-print ink anytime needed, the concentration of the three main compounds used to prepare the hydrogel were tested, namely methacrylated sodium alginate (MASA), ι-Carrageenan (CA) and carboxyl-methyl cellulose (CMC). The original protocol for the preparation of hydrogel bioink, which was revised as a result of the following experiments, suggested a range of concentrations (1 – 2%) for the aforementioned compounds, leading to variations in the properties of the final product. The tests conducted were focused on optimising the bioink preparation process so that the characteristics of viscosity, printability and stability after

photo-crosslinking would be consistent enough to allow for the standardisation of every other step in the production of 3D printed biofilm and focus on other aspects of the experiments' setup. The final version of the protocol can be found in section **3.7 Preparation of hydrogel bio-ink (bioink)**.

Batches of bioink were prepared in two 24-well plates (P1, P2) with increasing concentrations of MASA from top to bottom and increasing equal concentrations of CA and CMC from left to right. The setup used is shown in Table 4. The bioink was visually inspected to observe how homogeneous they were, and some candidates were selected for further inspection in terms of printing suitability. To these candidates 110 μ l of the photo-crosslinking mixture described previously in section **3.4 Photo-crosslinkers preparation** and 130 μ l of bacterial culture corresponding to a final OD₆₀₀ of 0.1 were added. After manually homogenizing, these were loaded into a 5 ml pressure printing cartridge to be printed into cylinders at 70 kPa and then photo-crosslinked overnight by exposure to green light.

The experiment showed that adjusting MASA concentration had no effect on the final viscosity of the ink, so it was kept at the highest value (2% [w/V]) in the final version of the protocol. Columns 1 to 3 corresponding to CA and CMC concentrations of 0 – 1%, showed a very soft gel, while columns 4 to 6 corresponding to concentrations of 1.5 – 2.5% did not result in a homogenous gel, as it became too stiff to allow mixing either by shaking or magnetic stirring. This phenomenon can be seen in Fig. 10. The most visible changes in the hydrogel came from the addition of CA, both while preparing it, before adding the CMC, and after, when testing printability. Any well with concentrations of CA above 1.5% yielded an inhomogeneous or simply too stiff hydrogel that was not suitable for 3D printing, either because of irregular extrusion (or no extrusion at all) or too frequent clogging of the cartridge tip.

	P1	1	2	3	4	5	6		P2	1	2	3	4	5	6
MASA [%]		1	1	1	1	1	1			1	1	1	1	1	1
CA [%]	A	0	0.5	1	1.5	2	2.5		A	1	1	1	1.5	1.5	1.5
CMC [%]		0	0.5	1	1.5	2	2.5			1	1.5	2	1	1.5	2
MASA [%]		1.5	1.5	1.5	1.5	1.5	1.5		B	1.5	1.5	1.5	1.5	1.5	1.5
CA [%]	B	0	0.5	1	1.5	2	2.5			1	1	1	1.5	1.5	1.5
CMC [%]		0	0.5	1	1.5	2	2.5			1	1.5	2	1	1.5	2
MASA [%]		2	2	2	2	2	2		C	2	2	2	2	2	2
CA [%]	C	0	0.5	1	1.5	2	2.5			1	1	1	1.5	1.5	1.5
CMC [%]		0	0.5	1	1.5	2	2.5			1	1.5	2	1	1.5	2
MASA [%]		2.5	2.5	2.5	2.5	2.5	2.5		D	2.5	2.5	2.5	2.5	2.5	2.5
CA [%]	D	0	0.5	1	1.5	2	2.5			1	1	1	1.5	1.5	1.5
CMC [%]		0	0.5	1	1.5	2	2.5			1	1.5	2	1	1.5	2

Table 4 – Composition of bioink tested in a combinatorial approach with optimised throughput, shown as two 24-well plates with three rows in each well corresponding to the three components of the bioink. Cells with yellow background fill in the range of concentrations suggested by initial protocol.

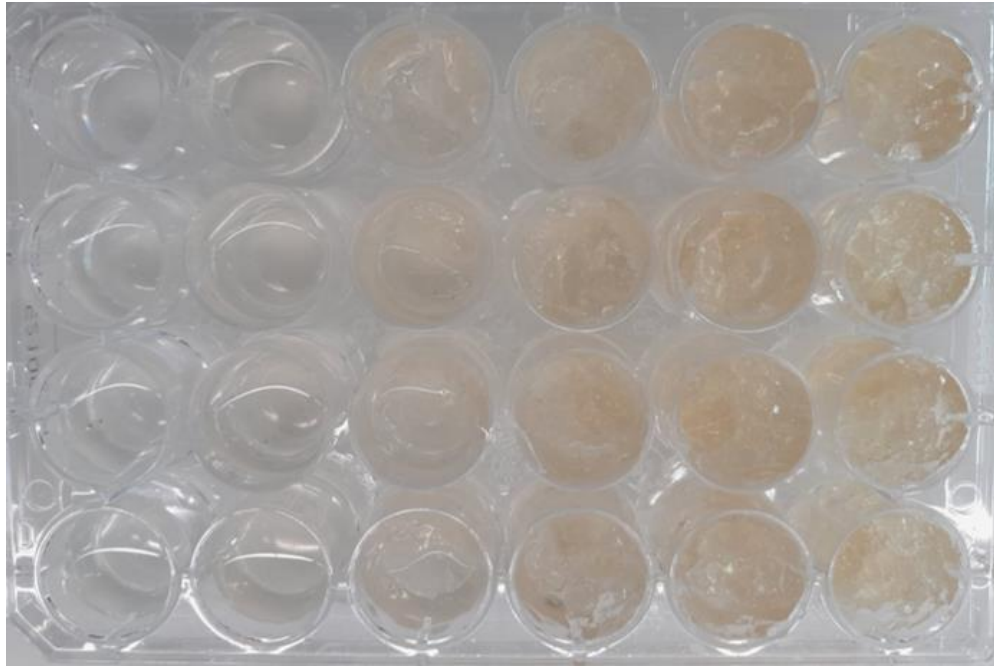


Fig. 10 – 24-well plate P1 with increasing MASA concentrations from top to bottom and increasing equal concentrations of CA and CMC from left to right. Alongside the colour, also the sturdiness of the bioink increases with higher concentrations of CA and CMC, while the homogeneity breaks between 1 and 1.5%.

The results also showed that CMC concentration, like MASA, did not have a relevant impact on final properties: if CA was able to dissolve and hydrogel became homogeneous in a reasonable amount of mixing/stirring time (below 5 hours) then the CMC would also be able to dissolve completely in a similar amount of time. For this reason, CA concentration was further inspected by preparing more batches of bioink with concentrations of CA ranging from 1 to 1.5% plus a control with 2% CA. This time a 6-well plate was used, increasing the volume of batches to 10ml.

	P3	1	2	3
MASA [%]		1.5	1.5	1.5
CA [%]	A	1	1.1	1.3
CMC [%]		1.5	1.5	1.5
MASA [%]		1.5	1.5	1.5
CA [%]	B	1.4	1.5	2
CMC [%]		1.5	1.5	1.5

Table 5 – Overview of 6-well plate P3 with different bioink samples and changing CA concentrations.

Resulting hydrogel that yielded failed prints even after many attempts of adjusting the pressure used were well A1 and B3, corresponding to CA concentrations of 1% and 2%. Some of the problems that arose with these two samples were printer tip clogging, filling space not being recognisable and first layer not sticking to the printing base (failed priming). Priming is important as the first layer gives stability to the rest of the print. If priming fails, the tip of the printer and the ink being extruded will drag the printed material, leading to shape alteration or disruption. An example of failed prints is shown in Fig. 11.

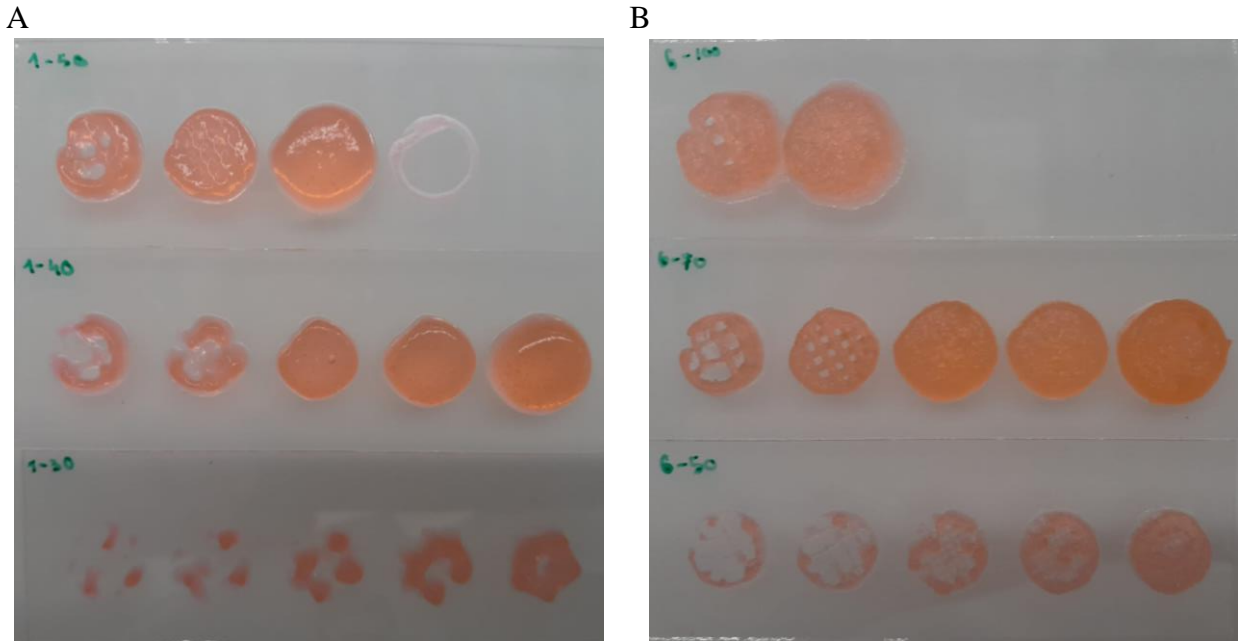


Fig. 11 – 3D printed series of 5 objects with decreasing filling spacing from 3 to 0.5 mm at 3 different pressure settings. A: The ink with the lowest concentration of CA (1%) printed at pressures of 50 kPa (top), 40 kPa (middle) and 30 kPa (bottom) shows similar behaviour to B: the ink with the highest concentration of CA (2%) printed at pressures of 100 kPa (top), 70 kPa (middle) and 50 kPa (bottom). Low pressures and filling densities led to interrupted priming, while high pressures or filling densities lead to faster extrusion than what specified in the software.

Excluding 1%, it was observed that low CA concentrations yielded a smoother gel, while higher CA concentrations led to a more grainy gel. Moreover, low CA concentrations led a continuous print of up to 10 objects without clogging the tip, while higher CA concentrations caused the tip to clog much more frequently. The final CA concentration to be inserted in the revised protocol was set to 1.3% based on the outcome of the printing trials. CMC concentration was set to 1.5% as it was faster to dissolve compared to 2%.

Having set the concentrations to have reliably printable bioink, the focus was shifted to the stability of photo-crosslinked hydrogel.

Another experiment was set up to assess the influence of MASA percentage on bioink viscosity, printability, as well as stability of the printed and photo cross-linked gels in water. The setup used was the following:

	P4	1	2	3
MASA [%]		1	1.5	1.63
CA [%]	A	1.3	1.3	1.3
CMC [%]		1.5	1.5	1.5
MASA [%]		1.75	1.88	2
CA [%]	B	1.3	1.3	1.3
CMC [%]		1.5	1.5	1.5

Table 6 – Overview of 6-well plate P4's samples with varying MASA concentrations and stable CA and CMC concentrations.

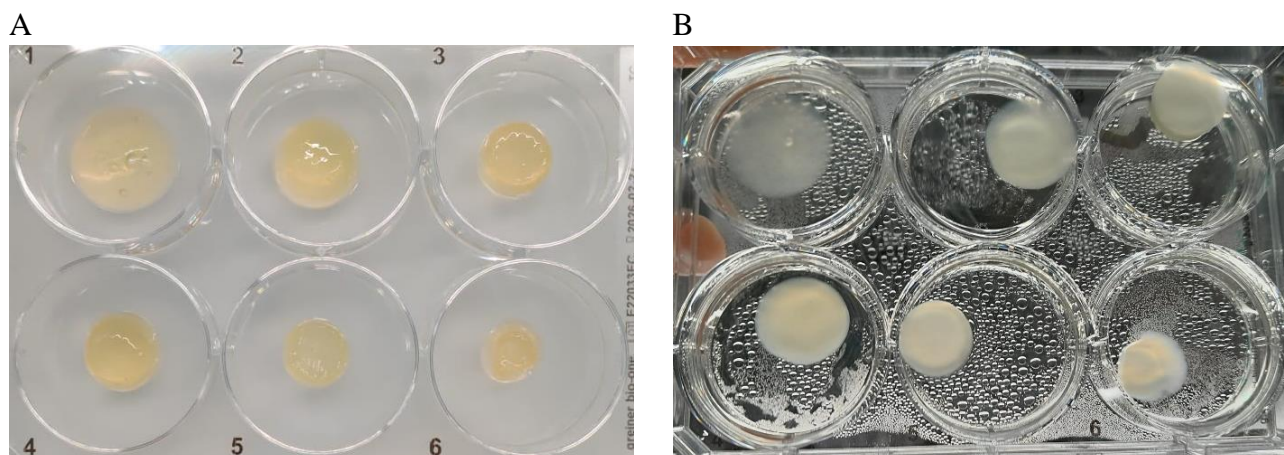


Fig. 12 – 3D printed gels with increasing MASA concentration of 1, 1.5, 1.63, 1.75, 1.88 and 2% right after photo crosslinking (A) and after 36 h incubation in water shown from below (B).

While printing, upon reaching the higher layers, the ink with less than 1.7% MASA yielded gelatinous masses with less distinct shape, a result comparable to shapes printed with too low CA concentrations or too high extrusion pressure. After incubation in water at 28°C, shaken at 700 rpm for 24h, any printed object that showed holes in its shape (well 1 and 4) was already soaking and showing signs of degradation. Conversely, gels with a MASA concentration of 1.75%, 1.88% and 2% w/V were still unaltered after incubation for two weeks in water at 28°C shaken at 700 rpm; even the superficial texture of the extrusion was still visible.

4.4 3D printing design and techniques development

The setup described in section 3.8 **Use of 3D printing in biofilm creation** was applied to investigate innovative techniques and shape designs. The aim was to improve the mechanical properties of the prints as well as to evaluate the optimal conditions for the coexistence of the two combined strains of bacteria (DSM14645 and JS666). The challenge to overcome was to create a system made out of bioink in which fixed bacteria of aerobic and anaerobic strains could survive and grow in a biofilm.

The first iteration of the design was a cube-in-cube model, in which a core of anaerobic bioink inoculated with DSM14645 would be encapsulated in layers of aerobic bioink inoculated with JS666. This setup was meant to provide close-to-anoxic conditions in the inner on the assumption that proper oxygen depletion was obtainable in the outer layers. The oxygen diffusing in from the environment was meant to be consumed by the JS666 in the outer shell at a fast enough rate to allow the anaerobes to survive. Challenging complications arose when designing the shape in the BioCAD software: the 3D bioprinter was able to extrude two materials at once from two separate cartridges so at first the design for the cube-in-cube model involved a simultaneous printing of the outer layers inoculated with JS666 and of the inner core inoculated with DSM14645. This way, the anaerobes were exposed to air for too long, being the printing of a full cube a 3-5 minutes long procedure, resulting in the death of the DSM14645. It became immediately evident that the anaerobic core needed to be added in anoxic conditions, therefore the next design tested was the same shape used before but deprived of the inner core. Limitations in the mechanical properties of the bioink became apparent as the cube could not be printed without a inner core: around halfpoint through the printing process the walls of the non-photo-crosslinked cube would collapse under its own weight. To solve this impediment, an attempt was made by using photo-crosslinking amidst printing to improve stability and increase the height limit of our objects without having to increase the width of the walls. Two solutions were adopted: stepwise photo-crosslinking and steady photo-crosslinking while printing. The first method tried was stepwise photo-crosslinking, consisting in interrupting the printing process every fixed amount of layers (5 in our case) with a 60 – 120 seconds exposure to green light to photo-crosslink

the material already printed, increasing its stiffness and providing improved steadiness. The long-term stability of the segmented prints was assessed by incubating the two cubic shapes seen in Fig. 13 in water at 30°C. As can be seen in Fig. 14, the segmented photo-crosslinking yields stable connections between the individually photo-crosslinked layers even under bacterial incubation condition for one week. No individually printed segments have been peeled off the object as a result of this experiment.

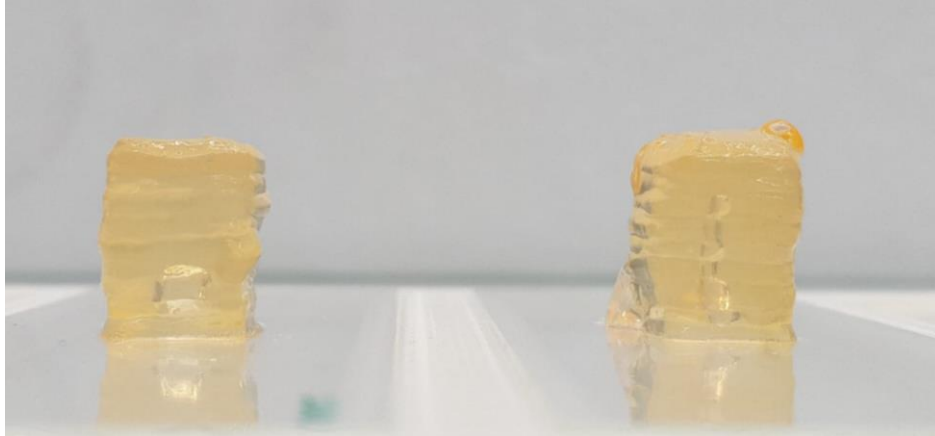


Fig. 13 – 3D printed cuboid (left) and egg (right) models of 50 layers each, after final photo-crosslinking of 30 min before incubation for stability assay.

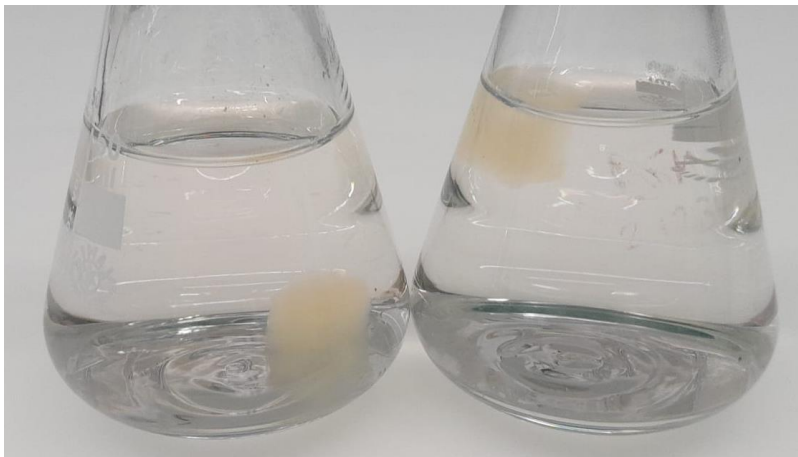


Fig. 14 – Long term stability test of stepwise photo-crosslinked prints in water. The cuboid (right) still floats due to the air bubble trapped inside while printing. The hollow cube (left) sank to the bottom but remained intact.

Since RegenHU software does not allow the user to pause and resume prints, stepwise photo-crosslinking was achieved by planning ahead during CAD design phase and creating multiple files to load into the machine for every step taken. Following that, the other approach adopted was steady photo-crosslinking while printing, which was done by setting the green LED close to the printhead pointing at the extrusion tip. This approach did not interrupt the printing process and allowed for faster printing sessions but achieved a lower level of improved stability.

Both methods guaranteed improved mechanical properties of the prints, making it possible to progress towards design-oriented approaches to assess other limits of the hydrogel bioink, such as which shapes could be printable and which could not, combinable versus single-print shapes, human aided versus full-automatized designs, as well as the survivability of the bacteria in such designs. The first one adopted was an improved version of the previously mentioned cube-in-cube design:

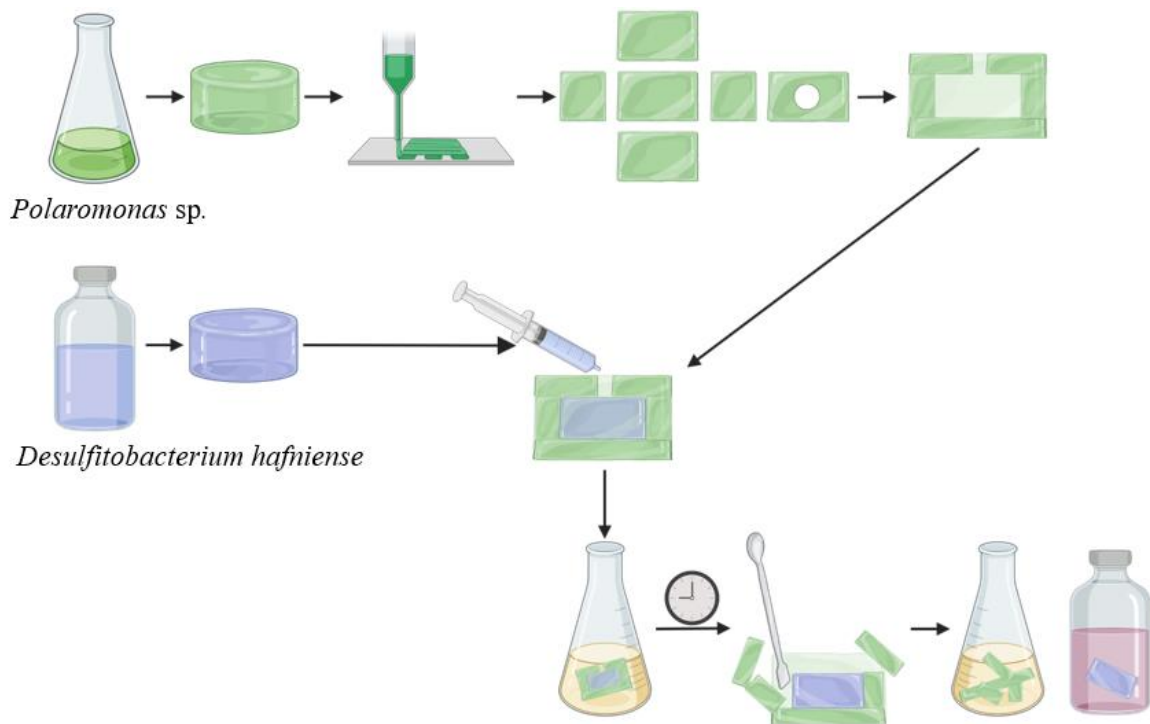


Fig. 15 – Schematics of the cube-in-cube design: the green ink, representing the aerobically inoculated portion of the print, the blue ink representing the anaerobically inoculated one. After an incubation period, the cube can be opened and the two original bioinks incubated separately to assess survivability of the bacteria.

This design consisted in printing 6 sheets of aerobic ink inoculated with *Polaromonas* sp. strain JS666 that would be then welded manually into a box shape upon photo-crosslinking using fresh non-photo-crosslinked ink. One of the objects would be printed with a hole, from which the anaerobic ink inoculated with *Desulfitobacterium hafniense* strain DSM14645 would be inserted manually in anoxic conditions.

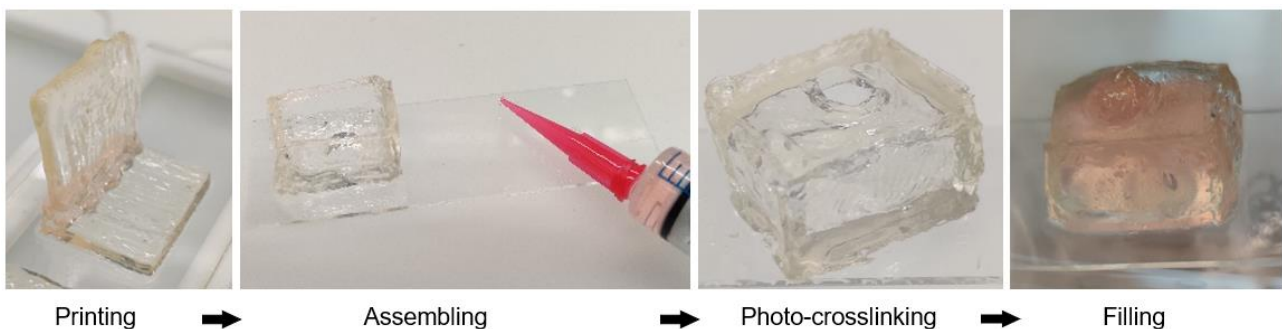


Fig. 16 – Steps in the preparation of an inoculated cube-in-cube sample, excluding a final photo-crosslinking step after filling.

After a period of 3 days of incubation in aerobic TSB/4 medium, the cube was cut open and the supposedly anaerobic core was incubated in anaerobic medium 1062 to verify that surviving DSM14645 bacteria were present. The OD₆₀₀ readings showed that anaerobes survived the process.

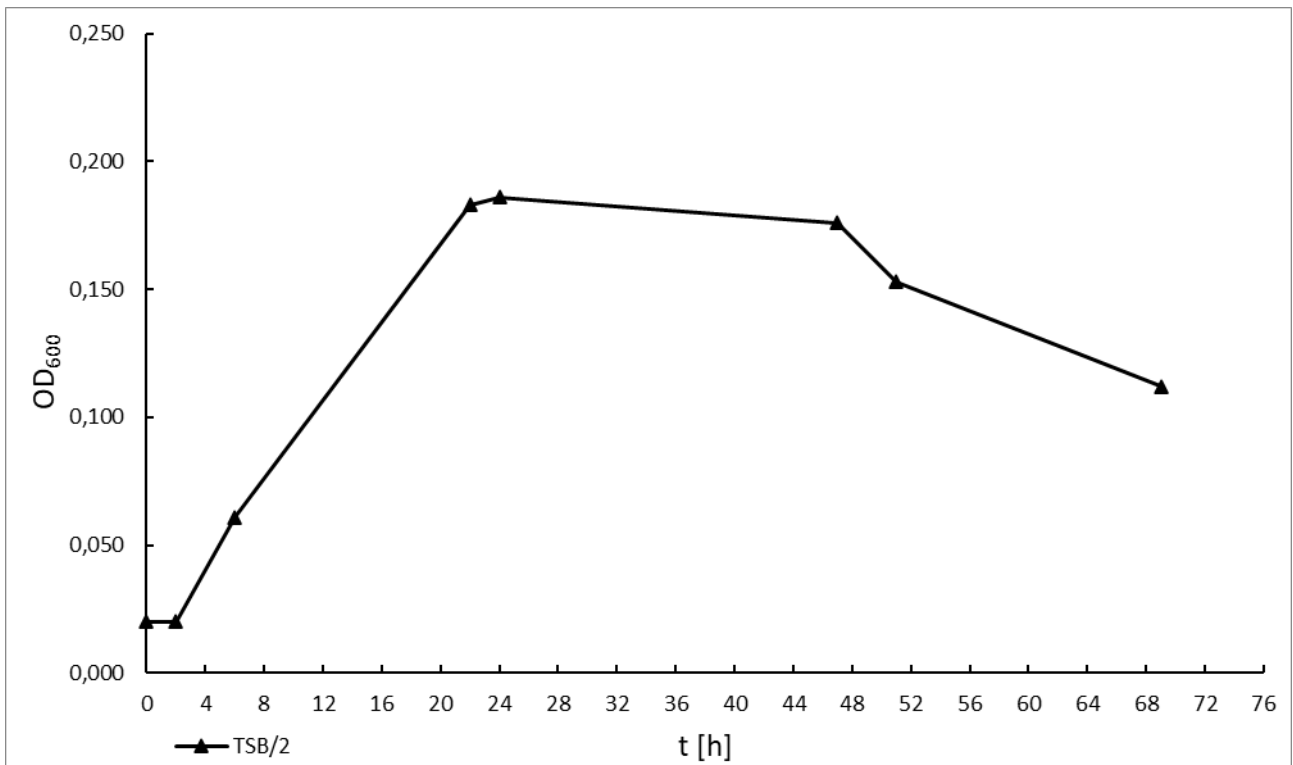


Fig. 17 – Growth curve of DSM14645 inoculated bioink in anaerobic medium 1062 coming from the core of a cube-in-cube print (DSM14645 in the core, JS666 on the outer layers) after 3 days of incubation in aerobic medium TSB/4 at 25 °C shaking at 110 rpm.

Other shapes tested were:

- Cylinder: two-pieces print consisting of hollow halves of a cylinder provided of a base, assembled manually into a whole;

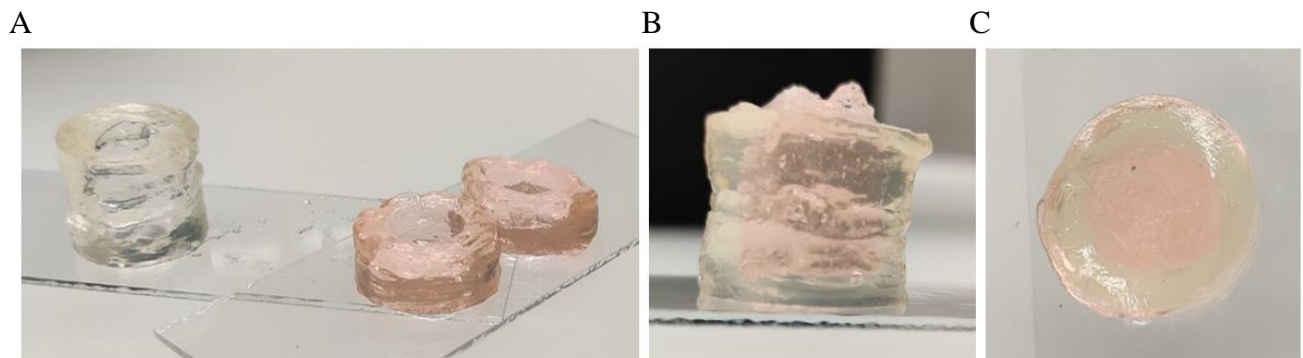


Fig. 18 – Cylindrical design print. The two pieces are seen pre (A, right) and post (A, left) assembling and photo-crosslinking. Front view (B) and top view (C) of the print with the addition of anaerobically inoculated bioink are also provided.

- Cone: single-piece print consisting of concentric layers of decreasing diameter stacked on a flat base

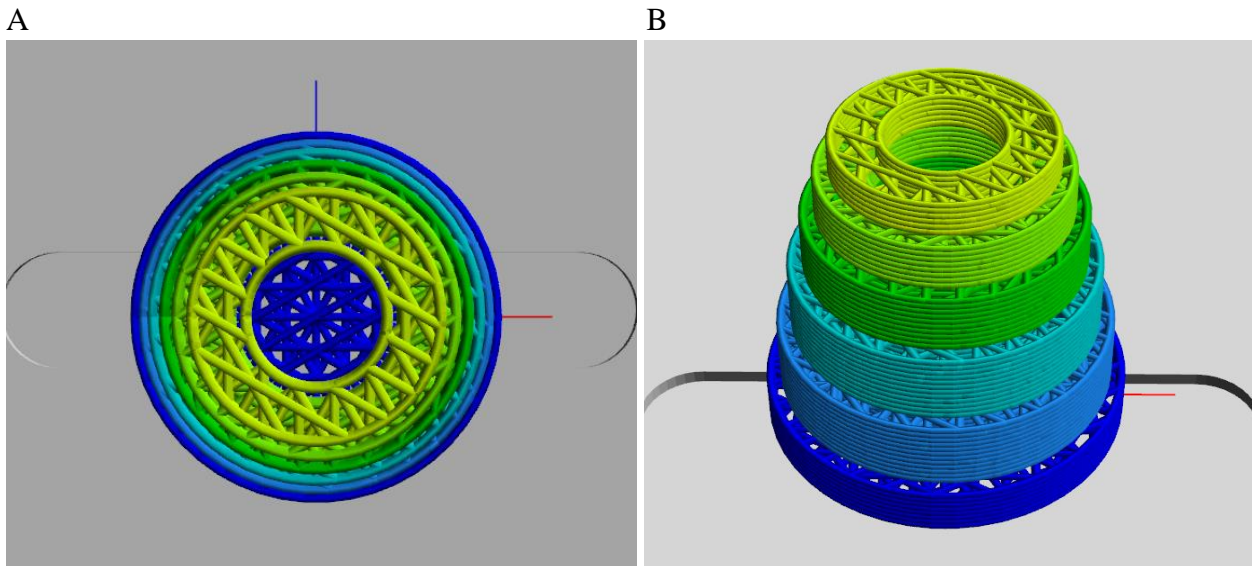


Fig. 19 – top view (A) and side view (B) of conical design in BioCAD (RegenHU 3D printing CAD software).

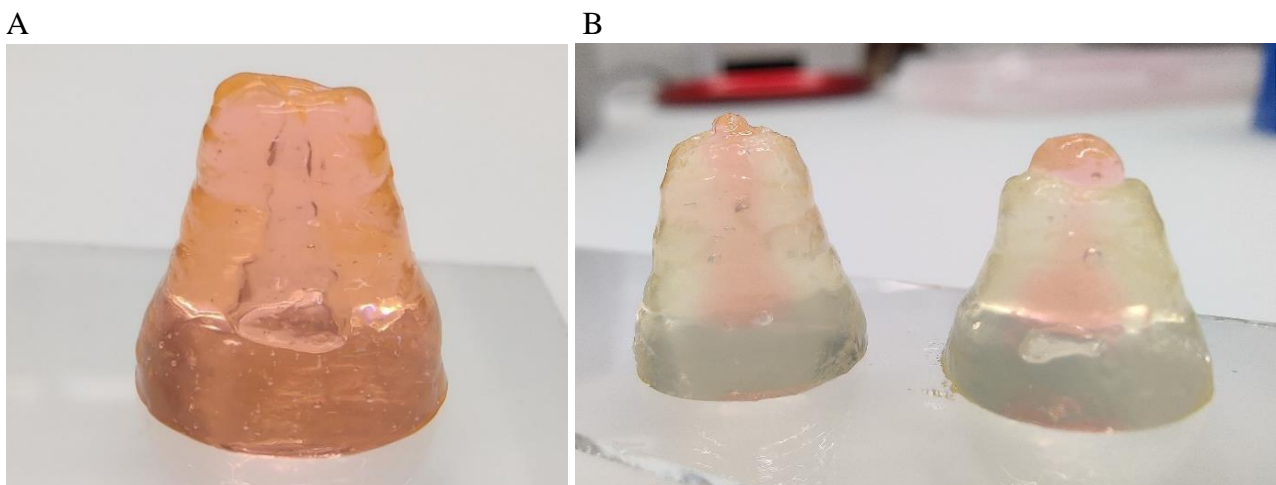


Fig. 20 – Conical prints empty before photo-crosslinking (A) and filled with non-photo-crosslinked anaerobic ink after photo-crosslinking the outside (B).

The second iteration of survivability test was conducted using the conical print design. The aerobic incubation was performed in low level nutrients media in order to simulate the environment in which a possible deployment of DSM14645 bacteria would have them to survive in. The assumed scenario was that of 3D printed bioink-based bioremediation of a contaminated aquifer, so an environment with low availability of nutrients. Media used were TSB diluted 1:2 and TSB diluted 1:20, the latter representing a low-nutrients environment. The duration of the incubation was 4 days instead of 3. After the incubation period the prints were again brought under anoxic conditions and opened as previously described, to incubate the core and assess survivability of anaerobes. Results are shown below:

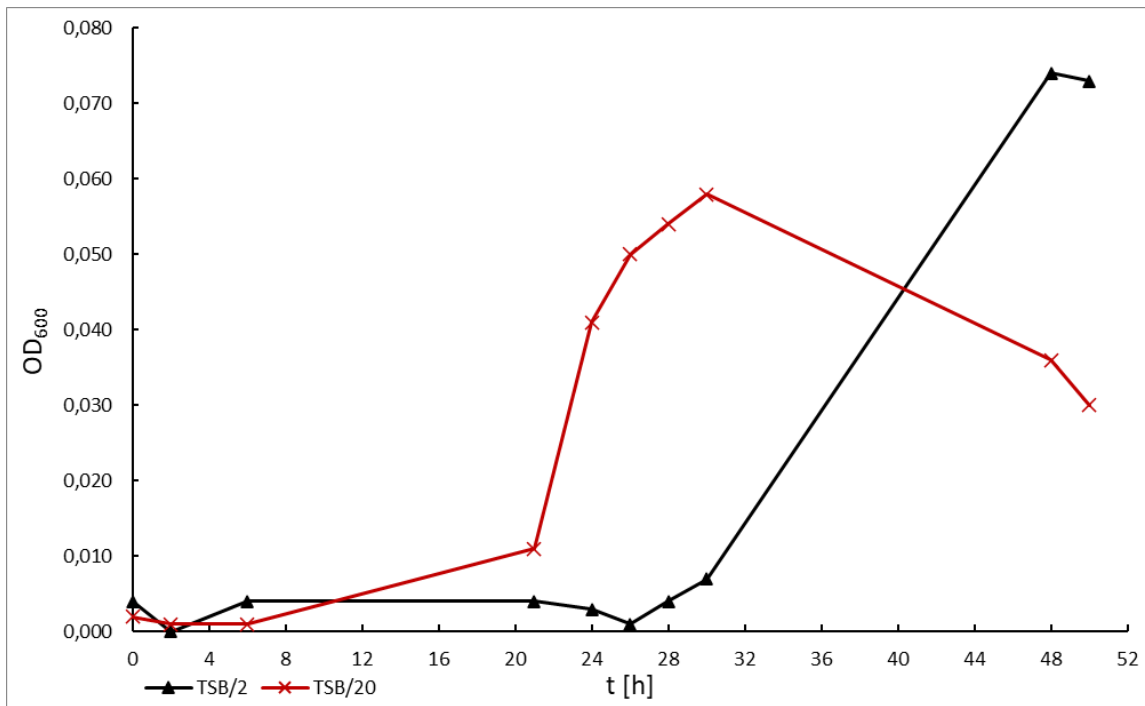


Fig. 21 – *OD₆₀₀ growth curves of anaerobically inoculated bioink in anaerobic medium 1062, coming from the core of conical prints inoculated with JS666 aerobic strain in the outer bioink layers and with DSM14645 in the inside layers after 4 days of aerobic incubation in diluted TSB media.*

In both cases, results showed survival of the anaerobes, which regrew after long lag phases of 20 and 30 hours for TSB/20 and TSB/2 respectively.

With the help of Dr. Joachim Köser, who shared his expertise on the utilisation of a laser scanning confocal microscope that was present at the facility where the project was being conducted, a few attempts at performing confocal microscopy on an anaerobically inoculated samples of bioink were made in the last months of the project. Further information about the samples preparation can be found in section **3.10 Confocal microscopy**. The resulting images are shown below:

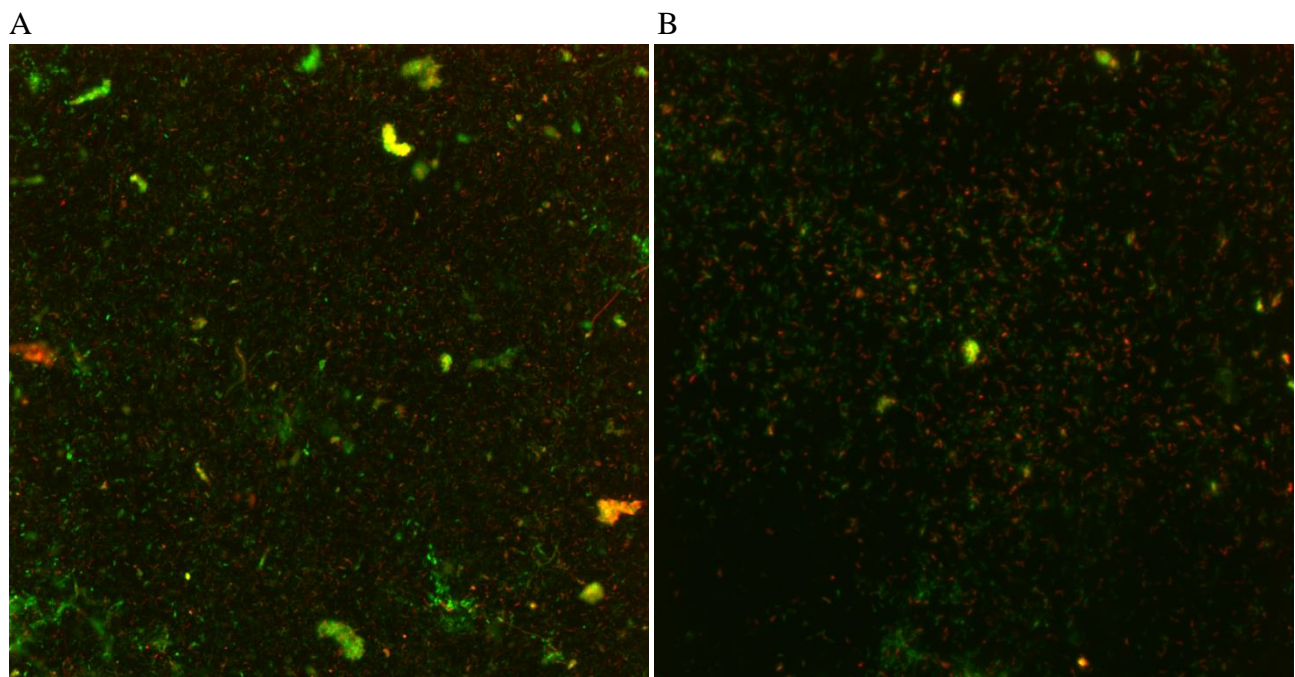


Fig. 22 – *Confocal microscopy of anaerobic bioink inoculated with stained DSM14645 bacterium. Pictures were taken from the centre of the sample (A) and from a less noisy region in the lower end (B) where individual bacteria can be seen better.*

4.5 PCE degradation assay

Samples prepared as described in section 3.9 Analytical measurements with GC-FID system underwent a degradation assay. The array of the different conditions employed are shown in Table 7; all the samples were kept incubating at 30 °C, non-shaking.

Sample type	Vial	Conditions
abiotic_print	B, K, Q	Abiotic bioink conical print in groundwater
sample_print	C, N, R	Inoculated conical print (JS666 outside, DSM14645 inside) in groundwater
PCES_bulk	D, H, I	DSM14645 liquid culture in groundwater
JS666_bulk	E, J, L	JS666 liquid culture in groundwater
both_bulk	G, O, P	DSM14645 and JS666 liquid culture in groundwater
TSB_bulk	A, F, M	DSM14645 and JS666 liquid culture in TSB medium

Table 7 – Sample preparation for PCE degradation assay.

Resulting readings from the GC-FID are shown below:

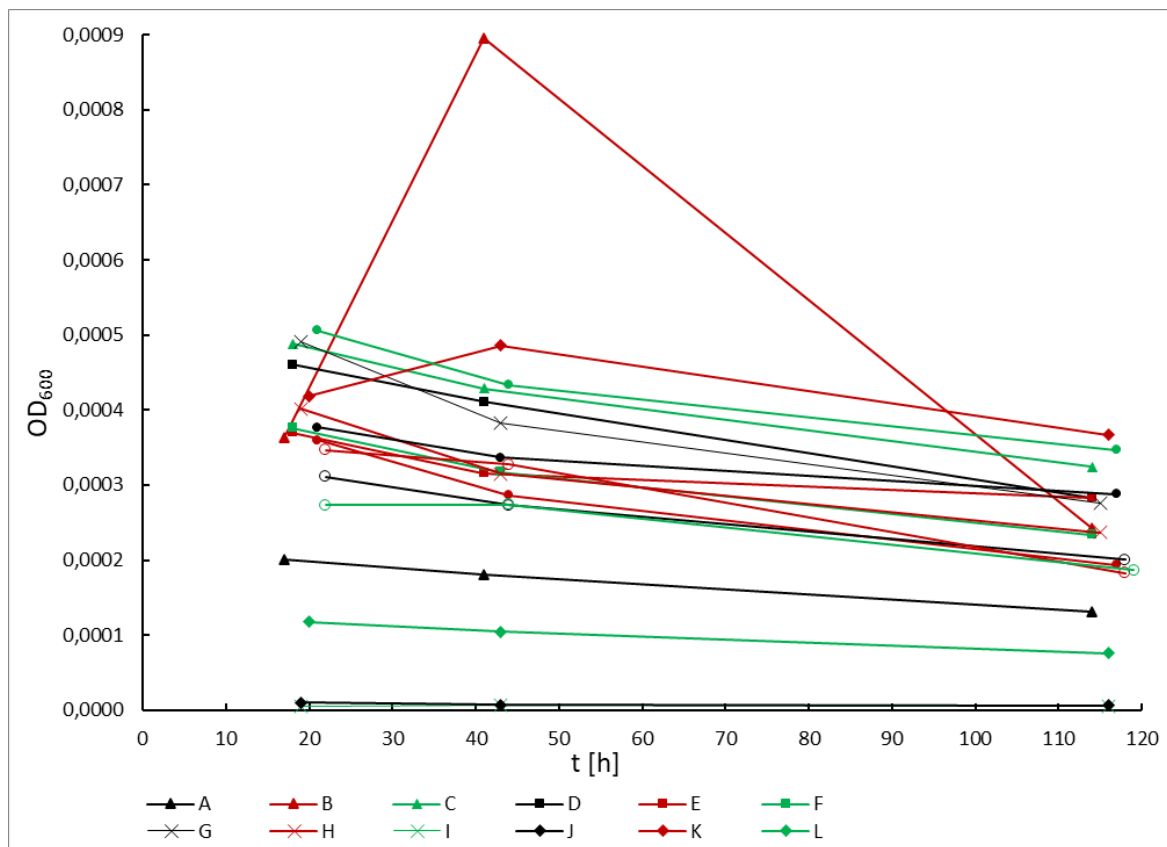


Fig. 23 – PCE concentration [mol/l] over time in all samples.

The PCE appears to be leaking from the PTFE coated stoppers, that were instead supposed to hold it in place, as seen from the concentration decreasing in every sample. This was assumed to be caused by the needle punctures that damaged the Teflon coat on the bottom side of the stopper. Further data is provided in Table 8.

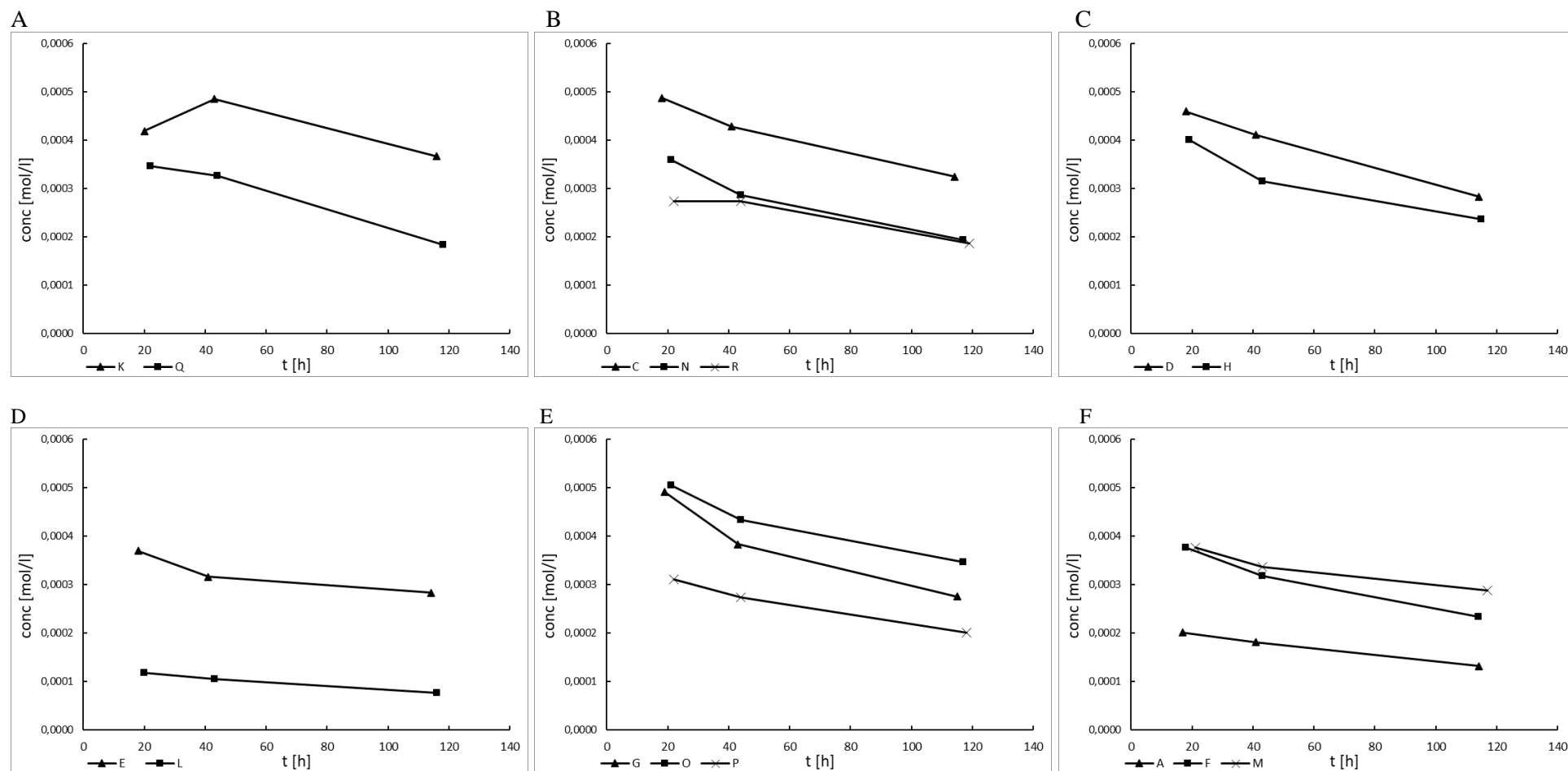


Fig. 24 – PCE concentrations in all samples grouped by sample type: abiotic_print (A), sample_print (B), PCES_bulk (C), JS666_bulk (D), both_bulk (E), TSB_bulk (F). Due to abnormally high or low values, samples B, I and J were discarded.

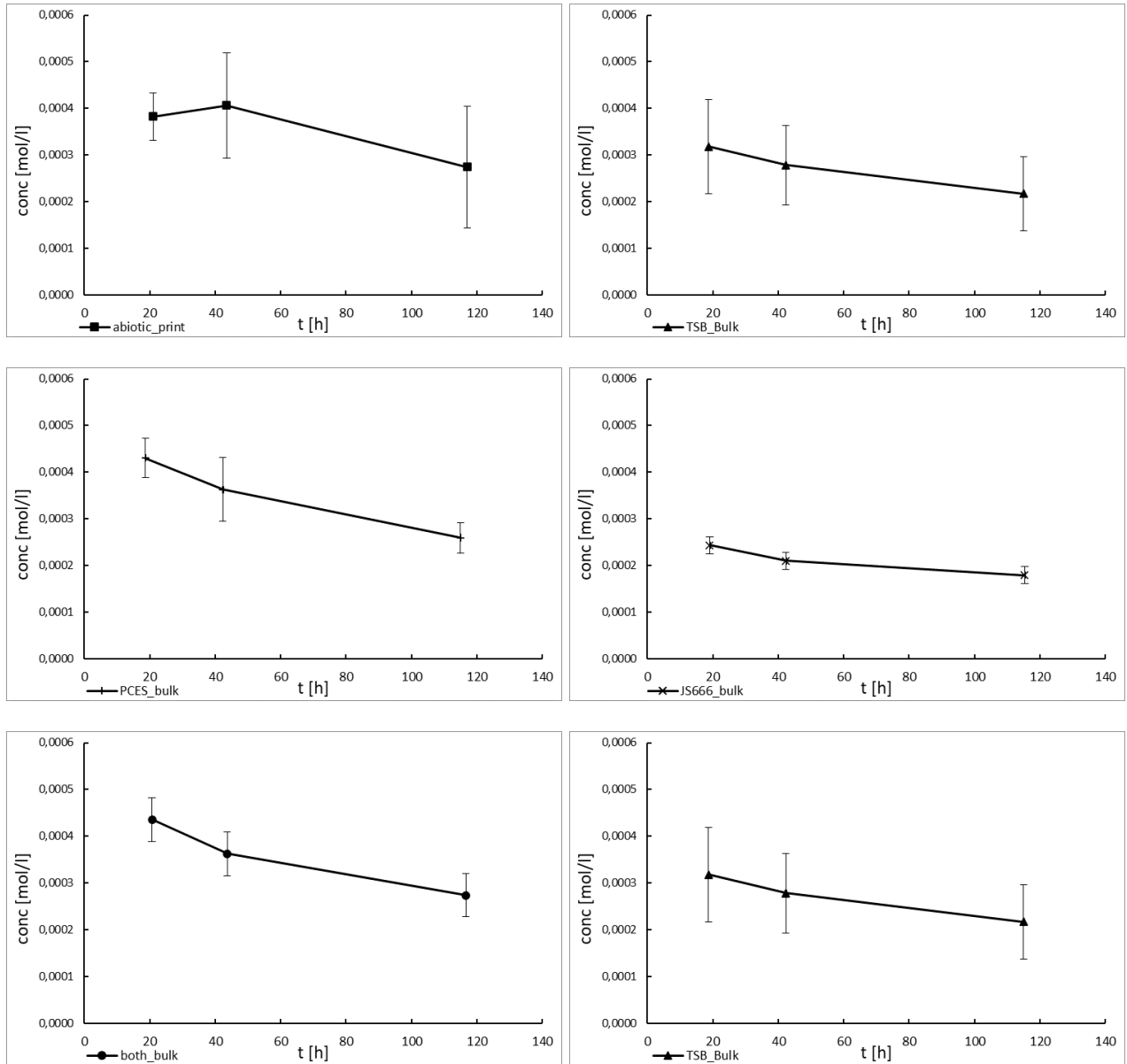


Fig. 25 – Averaged values of PCE concentration grouped by sample type. Error bars are calculated with standard deviations of single samples values.

TSB_Bulk			abiotic_print			sample_print			
t	avg. Conc	st.dev	t	avg. Conc	st.dev	t	avg. Conc	st.dev	
19	3,18E-04	0,00010141	21	3,83E-04	5,11882E-05	20	3,74E-04	0,000107858	
42	2,78E-04	8,4652E-05	44	4,06E-04	0,000112344	43	3,30E-04	8,58806E-05	
115	2,18E-04	7,9298E-05	117	2,75E-04	0,000130013	117	2,35E-04	7,77621E-05	
	-1,01E-04			-1,08E-04			-1,39E-04		delta depl.
	31,61%			28,23%			37,20%		depl. %
	-9,95E-07			-1,29E-06			-1,40E-06		slope
PCES_bulk			JS666_bulk			both_bulk			
t	avg. Conc	st.dev	t	avg. Conc	st.dev	t	avg. Conc	st.dev	
19	4,31E-04	4,1582E-05	19	2,43E-04	0,000178354	21	4,36E-04	0,00010827	
42	3,63E-04	6,8019E-05	42	2,10E-04	0,000149398	44	3,63E-04	8,18367E-05	
115	2,60E-04	3,2647E-05	115	1,80E-04	0,000146226	117	2,74E-04	7,29109E-05	
	-1,71E-04			-6,38E-05			-1,62E-04		delta depl.
	39,64%			26,21%			37,11%		depl. %
	-1,69E-06			-6,04E-07			-1,57E-06		slope

Table 8 – Average values of PCE depletion grouped by sample type (same used to draw Fig. 25) with color-coded data referencing to PCE depletion performance of each sample set (green being the best performing)

Confirmation runs have been done through GC-FID readings, to look for signs of degradation intermediates such as TCE or *cis*-DCE were found.

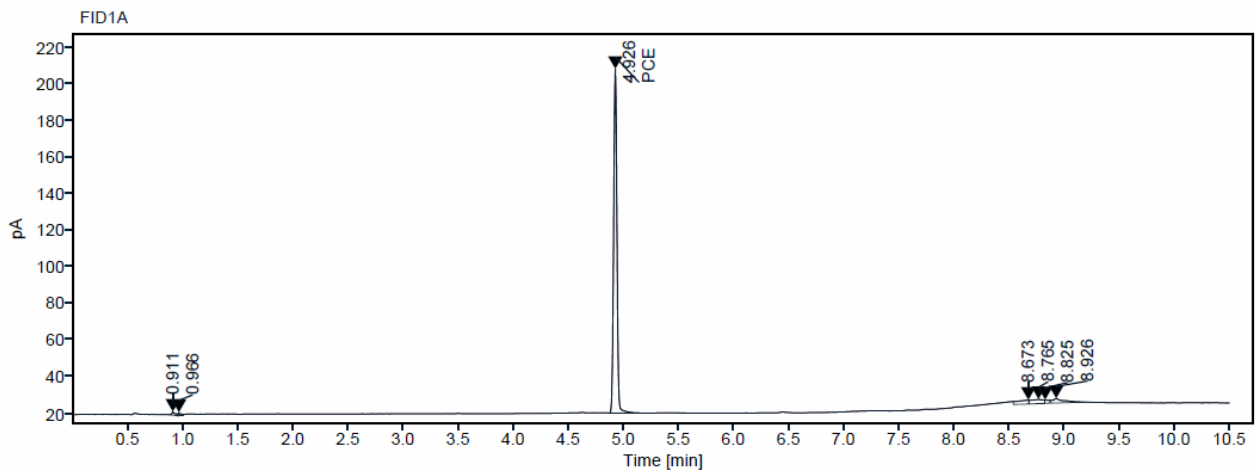


Fig. 26– GC-FID reading of sample H at t = 115h. PCE’s peak can be seen around 4.9 minutes but the rest of the curve is almost perfectly flat, with no traces of TCE or *cDCE* peaks, that should appear at 3.5 and 3.85 minutes respectively.

5. Discussion

5.1 Bacterial growth curve of DSM14645 in Medium 1062

The interpolation performed in Matlab output a rather common bacterial growth curve as expected, which suggests that both the incubation conditions and the medium of choice (Medium 1062) are appropriate choices for the optimal cultivation of the anaerobic strain employed. In the following months, while dealing with later sub-cultures, it was empirically verified that the growth asymptote for OD₆₀₀ readings was indeed around the 0.2 value. Cultures were able to survive stably in stationary conditions at that level of optical density for up to one week before dying off and forming precipitate of what was assumed to be dead cells.

5.2 Methacrylated Sodium Alginate synthesis analysis

The MASA synthesis analysis was conducted to create a reliable protocol in order to provide standardised conditions for further experiments and establish techniques for estimating the quality of MASA upon preparation. Without this, it would have been necessary to assess MASA quality by preparing a batch of hydrogel and observe its behaviour in 3D printed objects.

Unfortunately, the proposed models fit by STAVEX to the readout variables were unexpectedly poor, the best one being the one fit to the response variable of crosslinking ability, which reached an R² value of 0.91 and a corrected R²_c of 0.65. As can be seen in Fig. 6, the model suggests that MA concentration is the highest impacting factor among those analysed. This result came as expected, since the reaction in the photo-crosslinking process occurs between two double-bonds in the methacrylate group that was added to the alginate, with the Eosin-Y acting as a catalyst. Recommendations from literature regarding the methacrylation of alginate usually utilize a 10x or 20x MA volume excess compared to the alginate (Tahir and Floreani, 2022; Charron et al., 2016), to ensure that the alginate incorporates a large number of methacrylic groups. The washing steps with ethanol carried out at the end of the synthesis are specifically meant to remove such MA leftovers, otherwise these would be photo-crosslinking instead of the MASA, resulting in no mechanical improvements. Another factor that was discovered experimentally to play an important role in the synthesis was the cooling temperature during the reaction, even though the available thermoshakers used for mixing were not able to precisely control this parameter. This led us to work with temperatures of 8 - 12 °C during the addition of all components and a cooldown reaction temperature that went down to 8°C, instead of 4°C. As neither mixing speed nor reaction temperature were considered to be adjustable and both were kept as constant as possible across all samples, they were not considered to influence the outcome when inputting data into STAVEX. With the data gathered from the STAVEX analysis, the setup was updated to the one described in section **3.3 Synthesis of methacrylate modified sodium alginate (MA-SA)**. In particular, with the addition of an ice bath while adding MA and NaOH (points 2 and 3 of the protocol found in Appendix A) it became possible to reliably obtain a high quality MASA, despite the fact that most of the literature consulted did not specify a reaction temperature or performed the reaction at RT (Charron et al., 2021).

The improvements made in the MASA synthesis allowed us to have a reliably smooth gel with consistent viscosity, and consequently it became possible to move from pressure-driven extrusion with plastic tips to mechanical extrusion with metal tips. The abandoning of pressure-driven extrusion will be further discussed in the next paragraph.

Regarding the quality analysis of freshly prepared MASA with FTIR spectroscopy, the data obtained was sufficient to create a reference to compare with all subsequent batches, both to quickly assess if the MASA had been properly synthesised and to detect flaws in the product. The curves shown in Fig. 9 show a divergence in behaviour between pure MA and non-photo-crosslinking MASA. Before having the slopes of the intensities plotted out, our hypothesis for the failure to photo-crosslink was that MA leftovers from improper washings were crosslinking in competition with MASA. Instead, this data suggested that the reason behind the lack of photo-crosslinking might have been caused by an alternative competing reaction that turned the reactants into a different molecule, other than MASA. The additional peak located around wavelength 700 cm^{-1} could be indicating a C-H bond of a *cis*-alkene group, rather than the expected vinyl-group at a wavelength above 800 cm^{-1} in case of pure MA leftovers. Further investigation of the MASA synthesis reaction is due in order to complete the quality analysis by FTIR spectroscopy and to identify competing reactions that may affect the yield.

5.3 3D Bioprinting

Results from the batches displayed in Table 5 suggest that 1% and 2% CA concentrations were not suitable for printing, as problems would arise (independently of the pressure used) in the tip clogging, the filling space not being recognisable and the first layer not sticking (failed priming). The need for homogeneous prints with accurate filling came from the fact that the printed objects were supposed to resist for several days submerged in water, as mentioned in section **4.3 Influence of MASA, Carrageenan and Carboxyl-methyl cellulose on bioink properties**, as that was how they would be employed in case of a deployment during bioremediation of a contaminated aquifer. Instead, the necessity of mechanically stable prints, discussed in the successive section, arose with the need to print hollow objects. While working on the first iteration of the cube-in-cube design, since the anaerobic strain was being exposed to oxygen for too long while printing, the choice of creating first the outer shape and later injecting the anaerobic ink in anoxic conditions emerged as a logical consequence. Unfortunately, the old design could not be used, as the walls were collapsing due to the absence of an inner core to sustain their weight. Procedures adopted to preserve the box-shaped design involved optimizing priming to fit the behaviour of the 3D printer software, which was showing inconsistencies when prompted to print objects starting from different angulations, as well as reinforcing the walls by increasing their width, although this resulted in more time and materials needed for the production of the single prints and in less space on the inside to host the anaerobic ink.

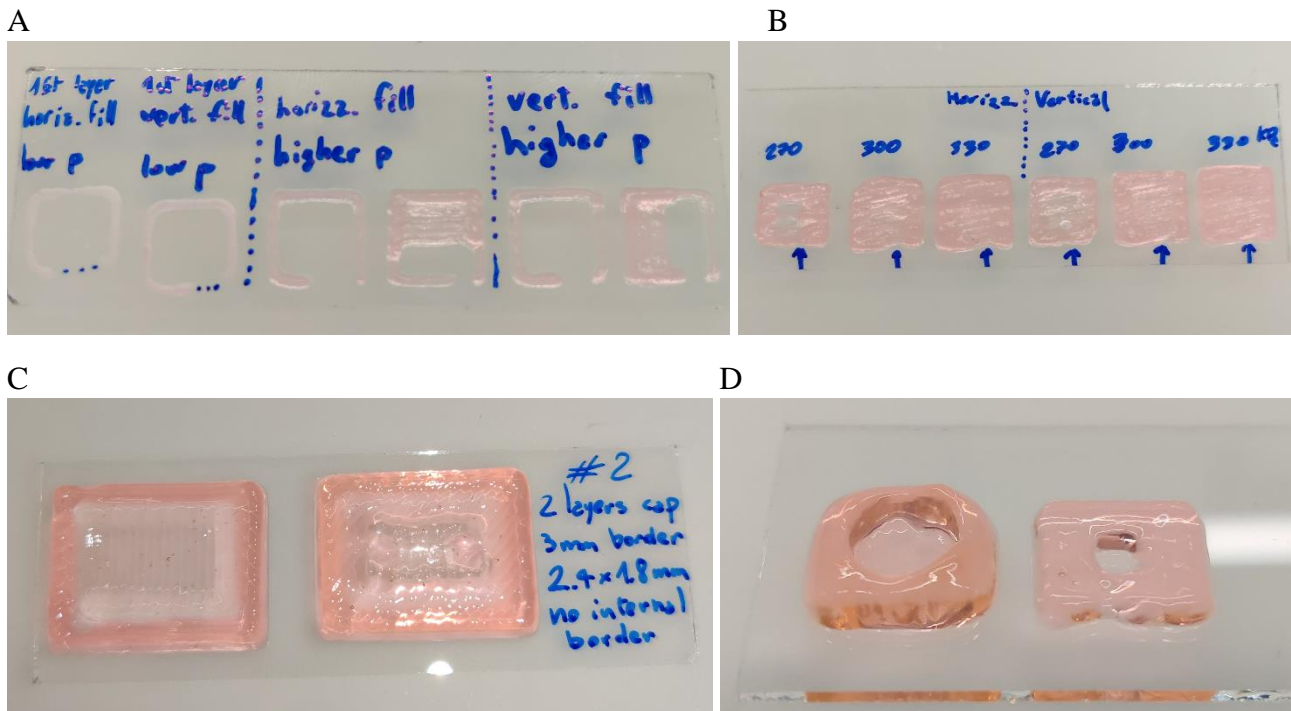


Fig. 27 – Instances of experiments on priming and texture detail (top) and hollow shapes (bottom). Different direction of filling (A) as well as different pressures (B) were tested to achieve efficient priming. The aim was to work around a software bug in the RegenHU software that made the printing of the first layer start with a gap on the bottom side of the square shape (highlighted with blue dots in A and pointed by the arrows in B). The consequences of improper priming were especially evident at low pressures. The print of hollow shapes was attempted with (C) and without (D) an increase of the walls' width, starting from the cube-in-cube design.

Following these studies on the print design, it became apparent that it was possible to print hollow shapes, but minor inconsistencies in the printer movements or in the bioink preparation would amplify greatly in the resulting print, making the whole process inefficient. For this reason, the attention was shifted towards combinable designs, the first of which was the one referenced in section **4.4 3D printing design and techniques development** as the improved version of the old cube-in-cube design. As it can be seen in Fig. 16, by printing the walls separately and photo-crosslinking them before assembling the shape, it was possible to create extremely precise and thin walls, that will still hold together once assembled thanks to them having to hold their weight only once photo-crosslinked. This served as a proof of concept to move on from cubical designs, as this new approach did not solve the inefficiency of printing, with a single print requiring close to an hour of work from the beginning of the printing to the last photo-crosslinking of the finished object. To further reduce the required time, it was necessary to reduce human handling of the print during the production process. Therefore, the shape was first changed from a cube to a cylinder, which was composed by only two pieces so required less time to assemble, as well as less accuracy. Furthermore, the previous design with six walls had twelve corners that needed to be welded with non-photo-crosslinked ink, all of which were likely points of failure that would often rupture during the injection of the core bioink. By having only one junction point and a simpler shape, the cylinder

proved to be a huge improvement over previous design, both mechanically and logistically. Further progress could only be obtained by removing the last junction of the cylinder, but it was impossible to print the perforated top without it collapsing. A working method to print a shape with a hole on top was to print sloped walls that would gradually get closer as the printing progressed, so the cylinder was abandoned in favour of the cone design. At this point, the need for improving bioink stability and therefore the integration of photo-crosslinking during the printing process became the top priority, as the achievable slopes and thicknesses of the walls were strictly dependant on the strength of the hydrogel.

An obstacle encountered while printing, in particular while using stepwise photo-crosslinking, was how time-consuming the process was due to the 3D printer inability to pause and resume the printing process. The method succeeded in increasing stability while printing and created prints that performed well in the water stability test seen in Fig. 14, which shows great adherence of independently photo-crosslinked layers as no water managed to infiltrate inside the object on the right. Despite that, the extra time in which the intermediate prints were left photo-crosslinking was often enough to alter their dimensions due to the hydrogel drying in the air, resulting in the unprecise shapes seen in Fig. 13. The method was abandoned mainly because of this, along with the time concerns about poor scalability given by the software's limitations. Photo-crosslinking while printing was found to provide enough mechanical improvements to the bioink to allow for the printing of more accurate shapes, so the method was adopted from that point on. It's also important to mention that at this point, air pressure-based extrusion had already been replaced by mechanically-driven extrusion, as this method did not require to manually adjust the strength exerted on the cartridge and therefore yielded more consistent results.

The advantages of printing with the conical design were mainly logistical, as fissures in the outer layers would still occasionally happen in case too much anaerobic ink was added or if the air in the hollow core of the print could not escape while filling it. On the other hand, being the cone a single-piece print, the printer could be set running while other tasks were being performed, such as cleaning or gathering equipment for another experiment, saving time over previous designs. This new design was the first one to remove the need for the presence of a human operator except for when the print had to be put under the green LED for photo-crosslinking. Finally, the design was scaled down to fit into a serum bottle, to facilitate further experiments regarding PCE degradation. Final conical prints had a base layer of 13 mm in diameter. This further increased the precision required by the 3D bioprinter during printing, making it impractical to use the 5 ml glass syringes for the printing process, which are less accurate than the 2.5 ml ones in extruding the bioink.

5.4 Bacterial survivability assay in 3D printed objects

The results from the survivability assay shown in Fig. 17 represented an important step in validating 3D printed bioink objects as means of transport for the delivery of living bacteria in a potential employment for bioremediation. The graph has been plotted with OD₆₀₀ growth observations of pieces of bioink incubating in medium 1062, which were coming from the core of a 3D printed object that had been incubating 3 days in aerobic conditions. The core of the object was consisting of anaerobic bioink inoculated with DSM14645, so the growth observed by anaerobically incubating said bioink was assumed to be DSM14645 bacteria.



Fig. 28 – Preparation of survivability assay to be performed on external walls of an assembled cube-in-cube print right before adding TSB medium (left) and of the anaerobic core in medium 1062 (right). The brownish-dark yellow colour of the bioink is attributed to the incubation period of 3 days in aerobic TSB media, which has a brown colour. The bioink in the picture had been chopped into pieces with a sterile spatula inside the glovebox.

The growth of anaerobes suggests that not only the exposure to oxygen during handling is not deadly to the microorganisms, but also that the hydrogel bioink is non-toxic for our specific strains of bacteria. Collateral death of the bacteria may have happened due to strain specific cytotoxicity of by-products or unreacted substances, or even from the photo-crosslinking process (Unagolla and Jayasuriya, 2020), but fortunately none of these factors seemed to have interacted negatively with the growth of DSM14645. It also appeared that the anaerobes could survive an incubation period of a few days in aerobic media TSB, likely thanks to the fact that the aerobic strain JS666 was depleting the oxygen coming from the environment fast enough to allow the anaerobes to survive. A compatible result was obtained by performing the survivability assay on the conical print design with less nutrient media and for 24 hours longer, as can be seen in Fig. 21. Here, the longer lag phase observed in the TSB/2-soaked sample was attributed to a higher survival rate of competing aerobic cells of JS666 that were on the outer layers, compared to the sample that had TSB/20. These survivors may have prevented the nutrients from reaching the core of the print and therefore prolonged the lag phase. Ultimately both samples went through exponential and stationary phase, suggesting a normal bacterial growth took place, but it's important to notice that the values of optical density reached were lower than those expected from DSM14645 in optimal conditions (Fig. 4). Such levels were only reached with the previous survivability assay, so the concentration of nutrients may have played a significant role in how the anaerobic bacteria hosted in the core of 3D bioprints behaved after the aerobes died. Further studies on the porosity of the bioink are recommended to further look into nutrients delivery to the core but also into the diffusion of oxygen and other chemicals or the bacterial inocula themselves. Finally, regarding the diffusion of the bacterial inoculum, the result of the confocal microscopy on samples of bioink suggested that the hydrogel would work in fact as a proper matrix for the creation of biofilm. This is because from Fig. 22-A it's noticeable how evenly distributed the bacteria are, both dead ones and living ones, although not much evidence was gathered regarding this matter.

5.5 PCE degradation in groundwater

An attempt has been made to estimate the PCE depletion potential of our 3D printed system. This was achieved by designing the setup described at the beginning of section **3.9 Analytical measurements with GC-FID system**, with the intent of having the two strains of bacteria act syntrophically on the degradation of PCE. Metabolites expected to be found were TCE, cDCE, VC and ultimately ethene.

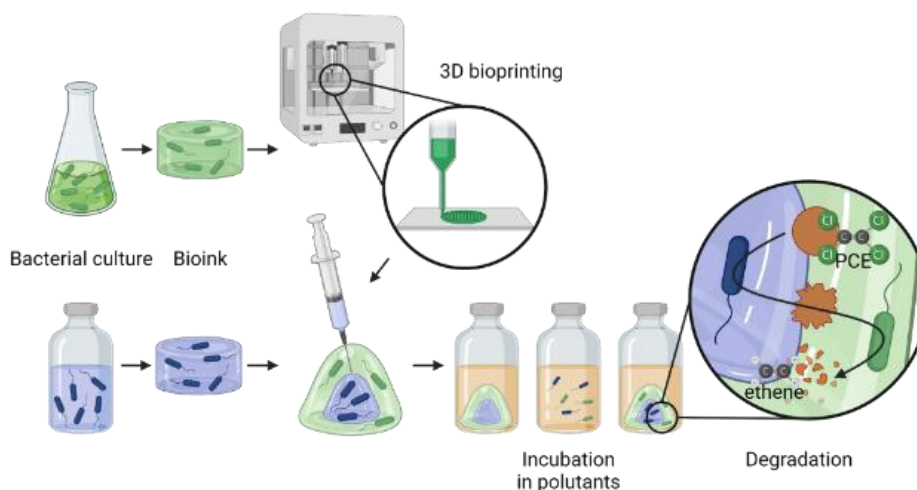


Fig. 29 – Schematical representation of experiment for PCE depletion potential investigation using 3D bioprinting of the conical print design to produce a syntrophic anaerobes-aerobes bioink system. The pollutants are shown (right) to be diffusing to the anaerobic core and then back to the outside layers while being metabolized.

Due to time constraints the experiment had to be limited to 5 days of exposure time (120 hours), but the outcomes suggest that longer duration might be required to obtain enhanced results or at least to rule out potential disruptors of such setup. As seen in Fig. 23 to Fig. 25, PCE concentration has been decreasing in all of the samples, including negative controls, suggesting that the pollutant was able to escape, presumably through the rubber of the PTFE coated stoppers. Upon confirming the lack of substantial progress in degradation after 5 days, the headspace vials have been opened to check the state of the caps, revealing considerable damage done by the syringe punctures.

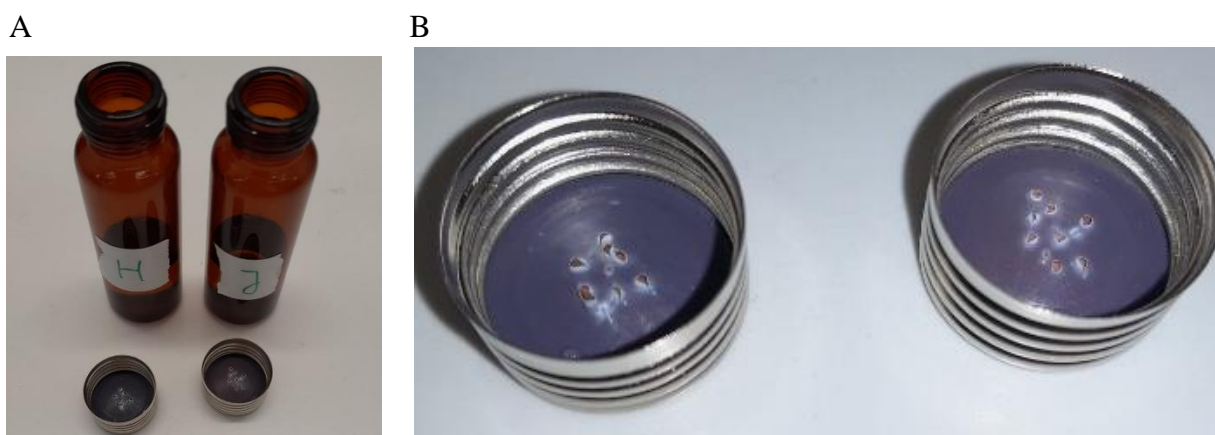


Fig. 30 – Headspace vials from sample H and J with caps removed (A) after 5 days of incubation, with close up of PTFE coating (B) exhibiting severe damaging done by the repeated punctures, which ended up exposing the brown rubber underneath.

Although data gathered in Table 8 appears to have shown a better performance of the samples that contained the degradation initiator DSM14645, these have been deemed not reliable due to the seemingly complete absence of degradation intermediates throughout all GC-FID readings, an example of which is shown in Fig. 26. The figure also shows how high the PCE peak still was at $t = 120$ hours, which was also considered a probable cause of no peaks of intermediates being identified, since being these in the noise range may have caused the machine to not properly detect their signal.

Consequently, a few more tests have been conducted to assess the issue of escaping PCE. GC-FID observations have been performed on serum bottles filled with deionized water and DSM14645 liquid cultures, both spiked with pure PCE and sealed with another kind of PTFE coated rubber stoppers (Wheaton® 20 mm butyl-isoprene blend flange straight-plug stoppers with PTFE coating). After approximately 500 hours, a consistent portion of the PCE was supposed to have escaped from the vials, since its concentration in the water-filled bottles was plunging daily. This was despite the fact that the number of punctures, and therefore the damage to the PTFE coating, was greatly reduced compared to the puncturing performed on the vials in the first setup. The results for the negative control, represented by the water-only bottles, are shown below:

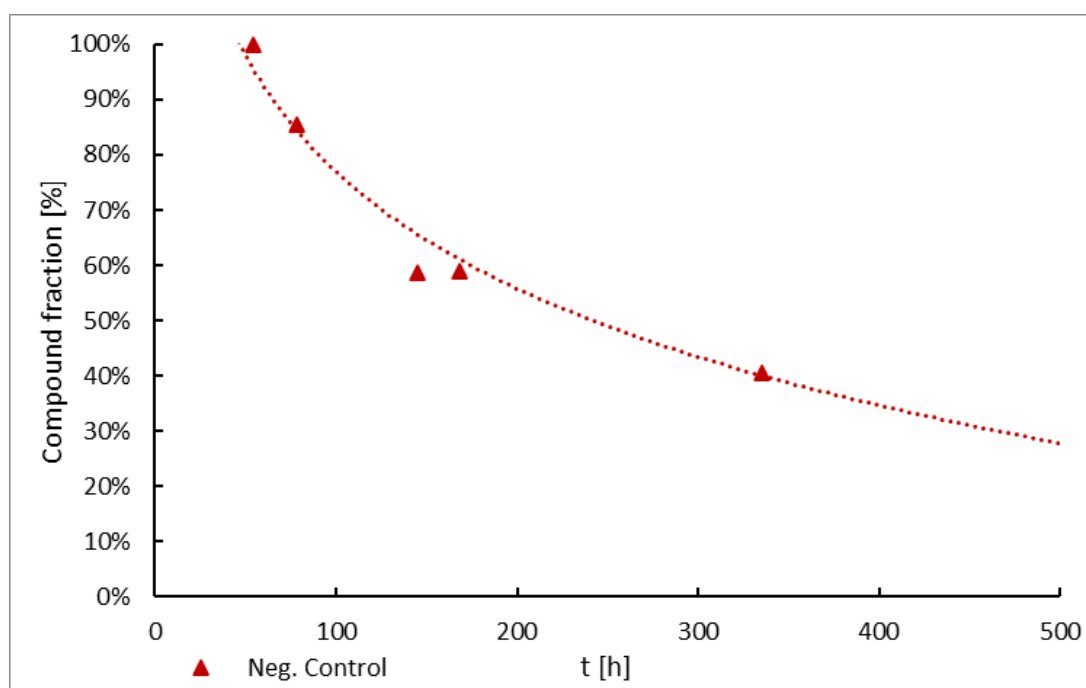


Fig. 31 – Headspace measurements with GC-FID on negative control expressed as percentage of PCE fraction. Dotted line represents a logarithmic curve fit to the data.

Results from the DSM14645 cultures showed instead a slower trend of PCE depletion, in contrast to what was expected from the positive controls, represented by 25 ml and 50 ml cultures of DSM14645 in optimal conditions.

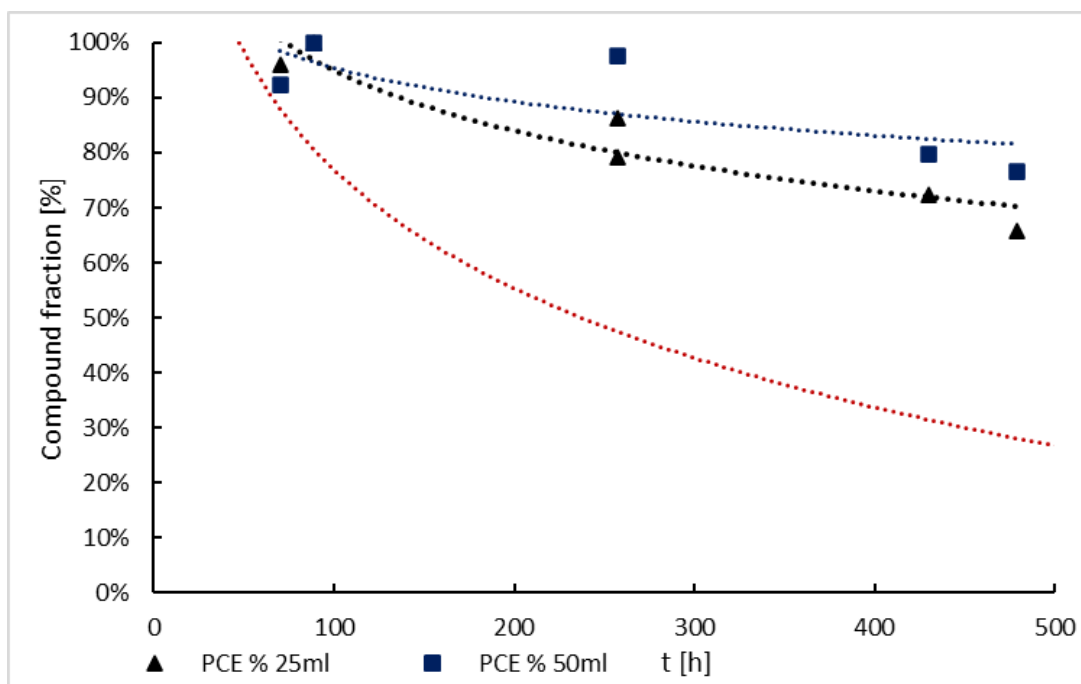


Fig. 32 – Headspace measurements with GC-FID on positive controls expressed as percentage of PCE fraction in 25 (black) and 50 (blue) ml cultures. The logarithmic fit from the graph in Fig. 31 (red) has been overlaid.

This trend difference may have been caused by the affinity between the pollutant and the liquid in which it was spiked; such affinity may have caused a faster release from the water to the headspace of the negative control compared to the active cultures, and therefore a faster escape through the rubber. Finally, part of this depletion was considered to be the work of bacterial metabolism, as presence of TCE was detected in the positive controls. Moreover, the fact that these miniscule quantities of TCE were only noticeable after 250 hours further supported the need for longer incubation times in PCE depletion potential related experiments.

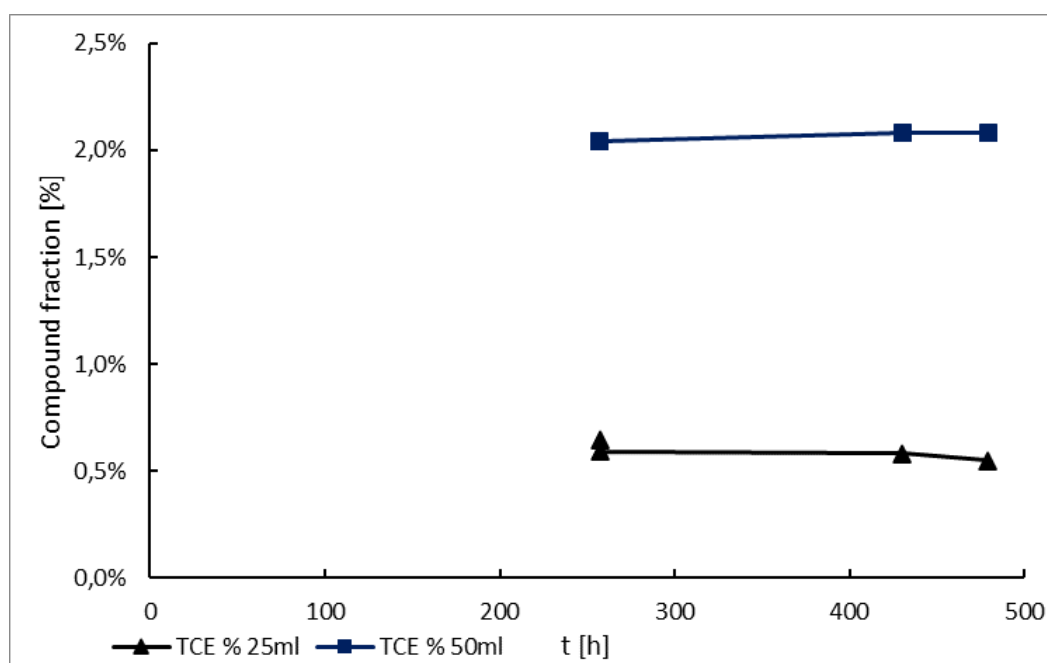


Fig. 33 – Headspace measurements with GC-FID on positive controls expressed as percentage of TCE fraction in 25 (black) and 50 (blue) ml cultures.

6. Conclusion

The data and the results collected with the experiments described so far further consolidate alginate hydrogel based bioinks as versatile and effective carrier materials to be used in microbial transport-related technologies, a prime example of which is bioremediation. The biocompatibility between the two strains of bacteria allows a variety of setups to be investigated, addressing both the quality of the material as well as the suitability of employed chemicals. Syntrophic systems provide an approach to tackle the described challenges, however their potential can only be fully exploited with further investigation and optimization. Currently, most of the technical challenges interfering with the consistent preparation of the processes have been solved, enabling higher throughput and consistency than what was possible before the laying down of protocols and techniques discussed in this thesis. The bacteria employed interacted non-destructively with each other while in the bioink, both in optimal conditions and in low nutrients cultures, and even though there is room for further optimization of such interactions, the groundwork for planning a more performance-oriented set up has now been provided. Degradation depletion potential of the bacteria is still considered unknown, given the many obstacles encountered in the experiment described in section **3.5 PCE degradation assay** and further discussed in section **4.5 PCE degradation in groundwater**. The use of gas chromatography is most likely the best option available for detecting a small volatile molecule like PCE, but different setups regarding the degradation conditions are yet to be explored.

During the course of the last experiments, the choice of process-specific conditions was the result of comparative evaluations performed by our team. The aim was to achieve a high degree of efficiency and automation in the production processes, in order to enable future designs of experiments to be more performance-oriented. One instance of employing this rationale was the adjustment of the original protocol for medium 1062 preparation, whose final version is included in **Appendix A**. For MASA synthesis, the importance of temperatures throughout the process is an important attribute to ensure a high quality of outcome, which is enabling higher accuracy during the production of 3D printed bioink objects, further facilitating the complexity of the shape design and the texture of the filling path.

Bioink structures allow a high freedom of design, which scales proportionally with the quality of the materials and the design used, as well as with the inventiveness and problem-solving abilities of the 3D-bioprinter operator. Moving forward, investigation of MASA synthesis would need to focus on the identification of possible competing reactions, whose presence was assumed based on FTIR analysis outcomes shown in Fig. 9. Such reactions not only affect the quality analysis performed with FTIR but could also decrease the yield of the synthesis process.

During the design phase of experiments, limitations of the used software and hardware instrumentation should be considered. In fact, in the context of 3D bioprinting not only physical and chemical limitations are present, but also mechanical and informatics related constraints can occur.

The performance of the specific model of 3D bioprinter used for this project is optimized for the production of small-sized detailed shapes. This requires the use of 2.5 ml syringes, for their improved stability over 5.0 ml ones, as well as metal printer tips instead of plastic ones, to increase precision and reduce clogging. Photo-crosslinking should be performed constantly while printing and up to 30 minutes once the shape is complete, in order to achieve maximum enhancement of mechanical properties of the bioink. Finally, mechanical extrusion is found to be more time-efficient and consistent compared to air-pressure extrusion; the BioCAD parameters employed for this procedure include feed rate of 15, layer thickness of 0.2 mm, no laser, no pressure, no cleaning and 0 strand start delay.

The study of degradation potential for PCE and its pathway intermediates of the examined strains of bacteria requires an improved setup that works around the obstacles encountered in this project. In particular, the escaping of PCE through the PTFE coated caps represents a major obstruction that needs to be either solved or accounted for. Further experiments should estimate the causes, as well as the relevance of such occurrence, since it would be theoretically possible to bypass it. However, the implications of such action on the results and their interpretation would be substantial. The rate of escape might be included as a baseline for all subsequent GC measurements, acting as a sort of normalisation for its influence. Alternatively, the PCE depletion rate might be measured in different ways, for instance by measuring pathway intermediates fractions in the headspace. Given the potential for PCE degradation of the employed system, efforts could now be focused on its bioremediating properties. Ultimately, incorporating 3D bioprinting in a broad multidisciplinary technology like bioremediation is likely to expand its use-cases. Within this framework, further investigation would be beneficial to both technologies.

7. Acknowledgements

This study was supported by the Electra Project, funded by the European Union's Horizon 2020 and the National Natural Science Foundation of China (NSFC). Experiments have been carried out at the Institute for Ecopreneurship (IEC) at the University of Applied Sciences and Arts of Northwestern Switzerland (FHNW). Fig. 15 and Fig. 29 were created with BioRender.com.

The author would like to express his sincere gratitude to Prof. Philippe Corvini and Prof. Fabio Fava for providing the opportunity to work on this project in the context of the IEC, which was a delightful experience. Great appreciation goes also towards Ana Dujmovic and Dr. Boris Kolvenbach for the support and insight they provided throughout the whole duration of the author's involvement in the project. The author also acknowledges the contribution of Dr. Marcel Suleiman for the contribution in anaerobic settings and in the revision of medium preparation protocols, Dr. Joachim Köser for the assistance in performing confocal laser scanning microscopy, Riccardo Perri for the support provided in the laboratory environment, all of which are deemed extremely valuable and appreciated.

8. Bibliography

Anna Dzionek, Urszula Guzik, and Danuta Wojcieszynska: Natural carriers in bioremediation: A review, *Electronic Journal of Biotechnology*, 23, 28–36, <https://doi.org/10.1016/j.ejbt.2016.07.003>, 2016.

Bolla, K. I. and Cadet, J. L.: Chapter 39 - Exogenous Acquired Metabolic Disorders of the Nervous System: Toxins and Illicit Drugs, in: *Textbook of Clinical Neurology (Third Edition)*, edited by: Goetz, C. G., W.B. Saunders, Philadelphia, 865–896, <https://doi.org/10.1016/B978-141603618-0.10039-6>, 2007.

FTIR Basic Organic Functional Group Reference Chart:

<https://www.thermofisher.com/blog/materials/a-gift-for-you-an-ftir-basic-organic-functional-group-reference-chart/>, last access: 10 February 2023.

Bradley, P. M. and Chapelle, F. H.: Biodegradation of Chlorinated Ethenes, in: *In Situ Remediation of Chlorinated Solvent Plumes*, edited by: Stroo, H. F. and Ward, C. H., Springer, New York, NY, 39–67, https://doi.org/10.1007/978-1-4419-1401-9_3, 2010.

Brown, R. A.: Chemical Oxidation and Reduction for chlorinated Solvent Remediation, in: *In Situ Remediation of Chlorinated Solvent Plumes*, edited by: Stroo, H. F. and Ward, C. H., Springer, New York, NY, 481–535, https://doi.org/10.1007/978-1-4419-1401-9_15, 2010.

Brusseau, M. L.: Chapter 15 - Subsurface Pollution, in: *Environmental and Pollution Science (Third Edition)*, edited by: Brusseau, M. L., Pepper, I. L., and Gerba, C. P., Academic Press, 237–259, <https://doi.org/10.1016/B978-0-12-814719-1.00015-X>, 2019.

Campbell, M., Suriya, L., Peceros, K., Sharma, P., Figtree, G., and Gentile, C.: Stem Cell Spheroids, in: *Encyclopedia of Tissue Engineering and Regenerative Medicine*, edited by: Reis, R. L., Academic Press, Oxford, 387–393, <https://doi.org/10.1016/B978-0-12-801238-3.65536-8>, 2019.

Charron, P. N., Fenn, S. L., Poniz, A., and Oldinski, R. A.: Mechanical properties and failure analysis of visible light crosslinked alginate-based tissue sealants, *J Mech Behav Biomed Mater*, 59, 314–321, <https://doi.org/10.1016/j.jmbbm.2016.02.003>, 2016.

Charron, P. N., Garcia, L. M., Tahir, I., and Floreani, R. A.: Bio-inspired green light crosslinked alginate-heparin hydrogels support HUVEC tube formation, *J Mech Behav Biomed Mater*, 125, 104932, <https://doi.org/10.1016/j.jmbbm.2021.104932>, 2021.

Chen, S.-K., Yang, H.-Y., Huang, S.-R., Hung, J.-M., Lu, C.-J., and Liu, M.-H.: Complete degradation of chlorinated ethenes and its intermediates through sequential anaerobic/aerobic biodegradation in simulated groundwater columns (complete degradation of chlorinated ethenes), *Int. J. Environ. Sci. Technol.*, 17, 4517–4530, <https://doi.org/10.1007/s13762-020-02792-z>, 2020.

Christiansen, N. and Ahring, B. K.: *Desulfitobacterium hafniense* sp. nov., an Anaerobic, Reductively Dechlorinating Bacterium, *International Journal of Systematic and Evolutionary Microbiology*, 46, 442–448, <https://doi.org/10.1099/00207713-46-2-442>, 1996.

Cichocki, J. A., Guyton, K. Z., Guha, N., Chiu, W. A., Rusyn, I., and Lash, L. H.: Target Organ Metabolism, Toxicity, and Mechanisms of Trichloroethylene and Perchloroethylene: Key

Similarities, Differences, and Data Gaps, *J Pharmacol Exp Ther*, 359, 110–123, <https://doi.org/10.1124/jpet.116.232629>, 2016.

Cooper, A. J. L. and Hanigan, M. H.: 4.17 - Enzymes Involved in Processing Glutathione Conjugates, in: *Comprehensive Toxicology (Second Edition)*, edited by: McQueen, C. A., Elsevier, Oxford, 323–366, <https://doi.org/10.1016/B978-0-08-046884-6.00417-6>, 2010.

Correia Carreira, S., Begum, R., and Perriman, A. W.: 3D Bioprinting: The Emergence of Programmable Biodesign, *Advanced Healthcare Materials*, 9, 1900554, <https://doi.org/10.1002/adhm.201900554>, 2020.

Drury, J. L. and Mooney, D. J.: Hydrogels for tissue engineering: scaffold design variables and applications, *Biomaterials*, 24, 4337–4351, [https://doi.org/10.1016/S0142-9612\(03\)00340-5](https://doi.org/10.1016/S0142-9612(03)00340-5), 2003.

Brief Profile - ECHA: <https://echa.europa.eu/brief-profile/-/briefprofile/100.004.388>, last access: 25 February 2023.

chlorinated hydrocarbon — European Environment Agency: <https://www.eea.europa.eu/help/glossary/eea-glossary/chlorinated-hydrocarbon>, last access: 4 March 2023.

Eicher, T. J.: CHAPTER 7 - Toxic Encephalopathies I: Cortical and Mixed Encephalopathies, in: *Clinical Neurotoxicology*, edited by: Dobbs, M. R., W.B. Saunders, Philadelphia, 69–87, <https://doi.org/10.1016/B978-032305260-3.50013-7>, 2009.

Ellis, D. E., Lutz, E. J., Odom, J. M., Buchanan, R. J., Bartlett, C. L., Lee, M. D., Harkness, M. R., and DeWeerd, K. A.: Bioaugmentation for Accelerated In Situ Anaerobic Bioremediation, *Environ. Sci. Technol.*, 34, 2254–2260, <https://doi.org/10.1021/es990638e>, 2000.

Perchloroethylene (PCE); Revision to Toxic Substances Control Act (TSCA) Risk Determination; Notice of Availability: <https://www.federalregister.gov/documents/2022/12/14/2022-27129/perchloroethylene-pce-revision-to-toxic-substances-control-act-tsca-risk-determination-notice-of>, last access: 25 February 2023.

Gao, W., Wang, H., Liu, Y., Tang, Q., Wu, P., Lin, T., Li, T., and Sun, D.: Sodium alginate-hydrogel coatings on extracorporeal membrane oxygenation for anticoagulation, *Front Cardiovasc Med*, 9, 966649, <https://doi.org/10.3389/fcvm.2022.966649>, 2022.

Henry, B. M.: Biostimulation for Anaerobic Bioremediation of Chlorinated Solvents, in: *In Situ Remediation of Chlorinated Solvent Plumes*, edited by: Stroo, H. F. and Ward, C. H., Springer, New York, NY, 357–423, https://doi.org/10.1007/978-1-4419-1401-9_12, 2010.

Holliger, C., Wohlfarth, G., and Diekert, G.: Reductive dechlorination in the energy metabolism of anaerobic bacteria, *FEMS Microbiol Rev*, 22, 383–398, <https://doi.org/10.1111/j.1574-6976.1998.tb00377.x>, 1998.

Jugder, B.-E., Ertan, H., Lee, M., Manefield, M., and Marquis, C. P.: Reductive Dehalogenases Come of Age in Biological Destruction of Organohalides, *Trends in Biotechnology*, 33, 595–610, <https://doi.org/10.1016/j.tibtech.2015.07.004>, 2015.

- Ke, Z., Obamwonyi, O., Kolvenbach, B., Ji, R., Liu, S., Jiang, J., and Corvini, P.: Insights into the applications of 3D bioprinting for bioremediation technologies, *Sheng wu gong cheng xue bao = Chinese journal of biotechnology*, 37, 3475–3486, <https://doi.org/10.13345/j.cjb.210427>, 2021.
- Koblitz, J., Halama, P., Spring, S., Thiel, V., Baschien, C., Hahnke, R. L., Pester, M., Overmann, J., and Reimer, L. C.: MediaDive: the expert-curated cultivation media database, *Nucleic Acids Research*, 51, D1531–D1538, <https://doi.org/10.1093/nar/gkac803>, 2023.
- Kocaman, A. Y. and Asfuroğlu, K.: The genotoxic effects of perchloroethylene in human peripheral blood lymphocytes and the possible ameliorative role of α -tocopherol, *Environ Sci Pollut Res Int*, 28, 39576–39586, <https://doi.org/10.1007/s11356-021-13523-3>, 2021.
- Kuppusamy, S., Palanisami, T., Megharaj, M., Venkateswarlu, K., and Naidu, R.: In-Situ Remediation Approaches for the Management of Contaminated Sites: A Comprehensive Overview, in: *Reviews of Environmental Contamination and Toxicology Volume 236*, edited by: de Voogt, P., Springer International Publishing, Cham, 1–115, https://doi.org/10.1007/978-3-319-20013-2_1, 2016.
- Leeson, A., Beevar, E., Henry, B., Fortenberry, J., and Coyle, C.: *Principles and Practices of Enhanced Anaerobic Bioremediation of Chlorinated Solvents*, 461, 2004.
- Lendvay, J. M., Löffler, F. E., Dollhopf, M., Aiello, M. R., Daniels, G., Fathepure, B. Z., Gebhard, M., Heine, R., Helton, R., Shi, J., Krajmalnik-Brown, R., Major, C. L., Barcelona, M. J., Petrovskis, E., Hickey, R., Tiedje, J. M., and Adriaens, P.: Bioreactive Barriers: A Comparison of Bioaugmentation and Biostimulation for Chlorinated Solvent Remediation, *Environ. Sci. Technol.*, 37, 1422–1431, <https://doi.org/10.1021/es025985u>, 2003.
- Liu, Y., Xia, X., Liu, Z., and Dong, M.: The Next Frontier of 3D Bioprinting: Bioactive Materials Functionalized by Bacteria, *Small*, n/a, 2205949, <https://doi.org/10.1002/sml.202205949>, 2022.
- Lyon, D. Y. and Vogel, T. M.: 6.10 - Bioaugmentation as a Strategy for the Treatment of Persistent Pollutants, in: *Comprehensive Biotechnology (Third Edition)*, edited by: Moo-Young, M., Pergamon, Oxford, 119–131, <https://doi.org/10.1016/B978-0-444-64046-8.00341-4>, 2011.
- Major, D. W., McMaster, M. L., Cox, E. E., Edwards, E. A., Dworatzek, S. M., Hendrickson, E. R., Starr, M. G., Payne, J. A., and Buonamici, L. W.: Field Demonstration of Successful Bioaugmentation To Achieve Dechlorination of Tetrachloroethene To Ethene, *Environ. Sci. Technol.*, 36, 5106–5116, <https://doi.org/10.1021/es0255711>, 2002.
- Malik, J. K., Aggarwal, M., Kalpana, S., and Gupta, R. C.: Chapter 38 - Chlorinated hydrocarbons and pyrethrins/pyrethroids, in: *Reproductive and Developmental Toxicology*, edited by: Gupta, R. C., Academic Press, San Diego, 487–501, <https://doi.org/10.1016/B978-0-12-382032-7.10038-4>, 2011.
- McCarty, P. L.: Groundwater Contamination by Chlorinated Solvents: History, Remediation Technologies and Strategies, in: *In Situ Remediation of Chlorinated Solvent Plumes*, edited by: Stroo, H. F. and Ward, C. H., Springer, New York, NY, 1–28, https://doi.org/10.1007/978-1-4419-1401-9_1, 2010.
- Merceron, T. K. and Murphy, S. V.: Chapter 14 - Hydrogels for 3D Bioprinting Applications, in: *Essentials of 3D Biofabrication and Translation*, edited by: Atala, A. and Yoo, J. J., Academic Press, Boston, 249–270, <https://doi.org/10.1016/B978-0-12-800972-7.00014-1>, 2015.

- Nijenhuis, I. and Kuntze, K.: Anaerobic microbial dehalogenation of organohalides—state of the art and remediation strategies, *Current Opinion in Biotechnology*, 38, 33–38, <https://doi.org/10.1016/j.copbio.2015.11.009>, 2016.
- Nobre, M. M. M. and Nobre, R. C. M.: Soil vapor extraction of chlorinated solvents at an industrial site in Brazil, *Journal of Hazardous Materials*, 110, 119–127, <https://doi.org/10.1016/j.jhazmat.2004.02.045>, 2004.
- Ramadan, Q. and Zourob, M.: 3D Bioprinting at the Frontier of Regenerative Medicine, Pharmaceutical, and Food Industries, *Frontiers in Medical Technology*, 2, 2021.
- Rastogi, P. and Kandasubramanian, B.: Review of alginate-based hydrogel bioprinting for application in tissue engineering, *Biofabrication*, 11, 042001, <https://doi.org/10.1088/1758-5090/ab331e>, 2019.
- Rédei, G. P. (Ed.): American Type Culture Collection (ATCC), in: *Encyclopedia of Genetics, Genomics, Proteomics and Informatics*, Springer Netherlands, Dordrecht, 75–75, https://doi.org/10.1007/978-1-4020-6754-9_623, 2008.
- Rifai, H. S., Borden, R. C., Newell, C. J., and Bedient, P. B.: Modeling Remediation of Chlorinated Solvent Plumes, in: *In Situ Remediation of Chlorinated Solvent Plumes*, edited by: Stroo, H. F. and Ward, C. H., Springer, New York, NY, 145–184, https://doi.org/10.1007/978-1-4419-1401-9_6, 2010.
- Rosato, D. and Rosato, D.: 1 - OVERVIEW, in: *Plastics Engineered Product Design*, edited by: Rosato, D. and Rosato, D., Elsevier Science, Amsterdam, 1–45, <https://doi.org/10.1016/B978-185617416-9/50002-8>, 2003.
- Sale, T. and Newell, C. J.: Impacts of Source Management on Chlorinated Solvent Plumes, in: *In Situ Remediation of Chlorinated Solvent Plumes*, edited by: Stroo, H. F. and Ward, C. H., Springer, New York, NY, 185–216, https://doi.org/10.1007/978-1-4419-1401-9_7, 2010.
- Scott Sutton: *Measurement of Cell Concentration in Suspension by Optical Density*, 2006.
- Smeds, K. A. and Grinstaff, M. W.: Photocrosslinkable polysaccharides for in situ hydrogel formation, *Journal of Biomedical Materials Research*, 54, 115–121, [https://doi.org/10.1002/1097-4636\(200101\)54:1<115::AID-JBM14>3.0.CO;2-Q](https://doi.org/10.1002/1097-4636(200101)54:1<115::AID-JBM14>3.0.CO;2-Q), 2001.
- Stroo, H. F., Major, D. W., and Gossett, J. M.: Bioaugmentation for Anaerobic Bioremediation of Chlorinated Solvents, in: *In Situ Remediation of Chlorinated Solvent Plumes*, edited by: Stroo, H. F. and Ward, C. H., Springer, New York, NY, 425–454, https://doi.org/10.1007/978-1-4419-1401-9_13, 2010.
- Suthersan, S. S., Horst, J., Schnobrich, M., Welty, N., and McDonough, J.: *Remediation Engineering: Design Concepts*, Second Edition, 2nd ed., CRC Press, Boca Raton, 627 pp., <https://doi.org/10.1201/9781315367088>, 2016.
- Tahir, I. and Floreani, R.: Dual-Crosslinked Alginate-Based Hydrogels with Tunable Mechanical Properties for Cultured Meat, *Foods*, 11, 2829, <https://doi.org/10.3390/foods11182829>, 2022.

Unagolla, J. M. and Jayasuriya, A. C.: Hydrogel-based 3D bioprinting: A comprehensive review on cell-laden hydrogels, bioink formulations, and future perspectives, *Appl Mater Today*, 18, 100479, <https://doi.org/10.1016/j.apmt.2019.100479>, 2020.

Xing, Z., Su, X., Zhang, X., Zhang, L., and Zhao, T.: Direct aerobic oxidation (DAO) of chlorinated aliphatic hydrocarbons: A review of key DAO bacteria, biometabolic pathways and in-situ bioremediation potential, *Environment International*, 162, 107165, <https://doi.org/10.1016/j.envint.2022.107165>, 2022.

Appendix A – Protocols

- **Medium 1062 *D. hafniense***

KH ₂ PO ₄	0.20 g
NH ₄ Cl	0.25 g
NaCl	1.00 g
MgCl ₂ x 6 H ₂ O	0.40 g
KCl	0.50 g
CaCl ₂ x 2 H ₂ O	0.15 g
Trace element solution 141	10.00 ml
Na-resazurin solution (0.1% w/v)	0.50 ml

Distilled water	1000.00 ml
-----------------	------------

1. Dissolve ingredients
2. Heat on 200° with close cap until boiling (undo the cap a bit to decrease pressure)
3. Keep heating with untightened cap for 5-10 minutes
4. Sparge with N₂ while cooling down on ice
5. When at room temperature (RT), distribute into serum bottles (previously sparged with N₂ for 1 minute) and sparge for 3 minutes
6. Autoclave
7. Prepare all other solutions separately:

Na ₂ CO ₃	3.75 g
ddH ₂ O	20 ml
Autoclave	<u>200 µl / 25 ml</u>

Yeast extract	5 g
ddH ₂ O	20 ml
Autoclave	<u>200 µl / 25 ml</u>

FeSO ₄ x 7 H ₂ O	0.137 g
H ₂ SO ₄	0.13 ml
ddH ₂ O fill up to	50 ml
Filter-sterilize	<u>200 µl / 25 ml</u>

Seven vitamins 503 filtered	25 µl / 25 ml
Dilute 10x	<u>250 µl / 25 ml</u>

Na ₂ -fumarate	40.6 g
ddH ₂ O	50 ml
Filter-sterilize	<u>200 µl / 25 ml</u>

Na-pyruvate	28.1 g
ddH ₂ O	50 ml
Filter-sterilize	<u>200 µl / 25 ml</u>

Na ₂ O ₄ S ₂	0.75 g
Anoxic ddH ₂ O	20 ml

Mix and filter-sterilize in glovebox 10 µl /25 ml

8. Add in underscored concentrations to cultures under biosafety hood by injecting with 1-2 ml syringes
9. Adjust pH to 7.5 with 4-7 drops of filtered H₂SO₄ 5M

- **Seven vitamins solution 503:**

D(+)-Biotin	20.00 mg
Nicotinic acid	200.00 mg
Calcium pantothenate	100.00 mg
Pyridoxine hydrochloride	300.00 mg
Thiamine-HCl x 2 H ₂ O	200.00 mg
Vitamin B12	100.00 mg
p-Aminobenzoic acid	80.00 mg

Distilled water	1000.00 ml
-----------------	------------

1. filter-sterilize before use

- **Trace element solution 141:**

Nitrilotriacetic acid	1.50 g
-----------------------	--------

Distilled water	1000.00 ml
-----------------	------------

1. adjust pH to 6.5 with KOH

MgSO ₄ x 7 H ₂ O	3.00 g
MnSO ₄ x H ₂ O	0.50 g
NaCl	1.00 g
FeSO ₄ x 7 H ₂ O	0.10 g
CoSO ₄ x 7 H ₂ O	0.18 g
CaCl ₂ x 2 H ₂ O	0.10 g
ZnSO ₄ x 7 H ₂ O	0.18 g
CuSO ₄ x 5 H ₂ O	0.01 g
KAl(SO ₄) ₂ x 12 H ₂ O	0.02 g
H ₃ BO ₃	0.01 g
Na ₂ MoO ₄ x 2 H ₂ O	0.01 g
NiCl ₂ x 6 H ₂ O	0.03 g
Na ₂ SeO ₃ x 5 H ₂ O	0.30 mg
Na ₂ WO ₄ x 2 H ₂ O	0.40 mg

2. readjust pH to 7.0 with KOH

- **ATCC medium: 2329 TSB or TSA, 1/4 strength**

Tryptic Soy Broth	7.5 g
Agar (if needed)	15.0 g

Distilled deionized water	1000.00 ml
---------------------------	------------

1. Autoclave at 121 °C for 15 minutes.
- **Preparation of glycerol stock solution**
 1. Glycerol \geq 99.5 % (Sigma-Aldrich, G9012-500 ml)
 2. Dilute into Duran® Schott bottle with deionized water to an end concentration of 40 % [V/V] glycerol, autoclave to sterilize the solution
 - **Preparation of bacterial glycerol stocks (cryostocks)**
 1. Incubate liquid culture in standard medium (e.g. TSB ¼) in incubator at given temperature and shaking until late exponential phase ($OD_{600} > 1$)
 2. In biosafety cabinet, transfer liquid culture into 50 ml falcon tubes
 3. Centrifuge at 4'500 x g for 8 – 10 min at 4 °C
 4. Discard about 80 % of the supernatant
 5. Add same volume of previously prepared sterile glycerol stock solution
 6. Re-suspend pellet and mix gently to get homogenous suspension
 7. Aliquot 1 – 1.5 ml into cryogenic storage vials
 8. Store the cryogenic storage vials into the freezer at -80°C
 - **Defrosting**
 1. Remove corresponding cryogenic storage vial from freezer, store on ice while defrosting
 2. In biosafety cabinet, transfer 250 – 500 μ l of thawed cell suspension in fresh corresponding liquid growth media [50 – 100 ml] to incubate at given temperature and shaking
 - Put back remaining glycerol stock into – 80 °C freezer for re-use
 - **Synthesis of methacrylated alginate**
 1. Prepare a 2 % [w/V] solution of SA in a beaker – dissolve in 80 °C hot water (expected duration: > 30 min)
 2. Add MA with 20-fold excess based to the weight of SA, (e.g. 1 g SA = 20 ml MA)
 3. Adjust the pH to 8 with 5 molar sodium hydroxide (5M NaOH)

Note: Best results were achieved by adding 22-25 ml NaOH droplet wise by using a droplet funnel over a time period > 30 min, under strong stirring, while keeping the container cooled down in ice. Perform the additions of Point 2 and Point 3 under a chemical hood.
 4. Incubate the solution at 5 °C for 48 h under continuous stirring at >800 rpm

Note: Use overhead electrical stirrer to achieve strong turbulences, as the solution will get sticky and viscous. Seal the container to reduce the spreading of dangerous gasses.
 5. After the incubation, add ethanol absolute (volume 1:1), centrifuge the synthesized SA-MA by 9000 x g for 8 min and remove the supernatant. Wash the solution with ethanol absolute in excess at least four times to remove remaining methacrylic anhydride and other impurities.
 6. Remove the supernatant from the precipitated MA-SA (gel like, white) and let dry over night at RT
 7. Dried MA-SA is ready to use for hydrogel preparation
 - **HEPES Stock Solution (0.1 M, pH 7.4)**
 1. Add 2.38 g of HEPES to an appropriate beaker (100-200 ml beaker in this case).
 2. Add about 80 ml of deionized water to the beaker.

3. Add a stirring bar to the beaker and leave it on a stirring plate until completely dissolved (~1 min).
4. Start monitoring pH of the solution. It should be acidic (pH ~5).
5. Adjust pH = 7.4 by using NaOH solution
Caution: wear gloves, eye protection and exercise extreme caution with this solution
6. Once the pH of the solution is 7.4, add enough deionized water to raise the volume to 100 ml.
7. Filter sterilize (optional), and store in the refrigerator for up to 4 months or aliquot and freeze at -20 °C for future use.

- **HEPES Stock Solution (0.1 M, pH 7.4)**

1. Add 2.38 g of HEPES to an appropriate beaker (100-200 ml beaker in this case).
2. Add about 80 ml of deionized water to the beaker.
3. Add a stirring bar to the beaker and leave it on a stirring plate until completely dissolved (~1 min).
4. Start monitoring pH of the solution. It should be acidic (pH ~5).
5. Adjust pH = 7.4 by using NaOH solution
Caution: wear gloves, eye protection and exercise extreme caution with this solution
6. Once the pH of the solution is 7.4, add enough deionized water to raise the volume to 100 ml.
7. Filter sterilize (optional), and store in the refrigerator for up to 4 months or aliquot and freeze at -20 °C for future use.

- **Preparation of hydrogel bio-ink**

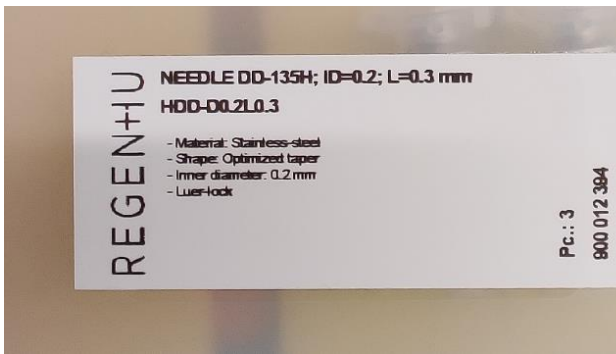
1. Dissolve MA-SA, CA and CMC in 80 °C hot water/media under roughly stirring (Use of overhead electrical stirrer recommended)
Note: Add every ingredient sequentially only after the previous one is dissolved
2. For “photo-crosslinkable” ink add the following components:
add 10 µL of 0.5% eosin (EY) in 1-vinyl-pyrrolidionen (VP) and 100 µL of 5.0 M triethanol amine (TEA) in HEPES per 2mL of 2% [w/V] solution of MA-SA and mix by hand until the ink becomes homogeneous in colour
Note: Reduce the water volume slightly by the volume of photo-crosslink initiators added to reach the desired final volume and concentrations
3. For biotic hydrogel: add inoculum and mix by hand until the ink becomes homogeneous

Appendix B – Images

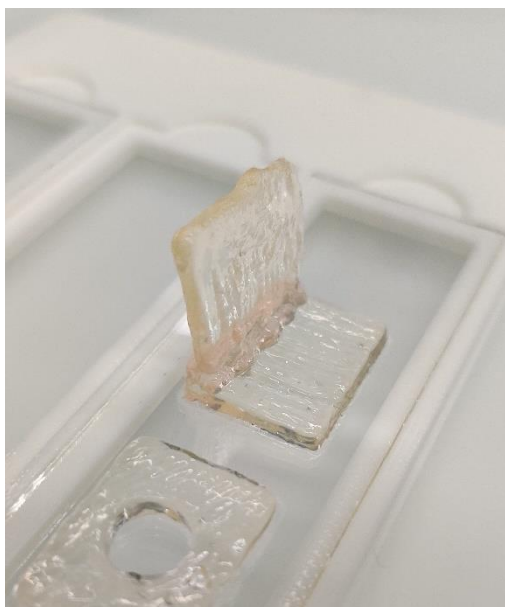
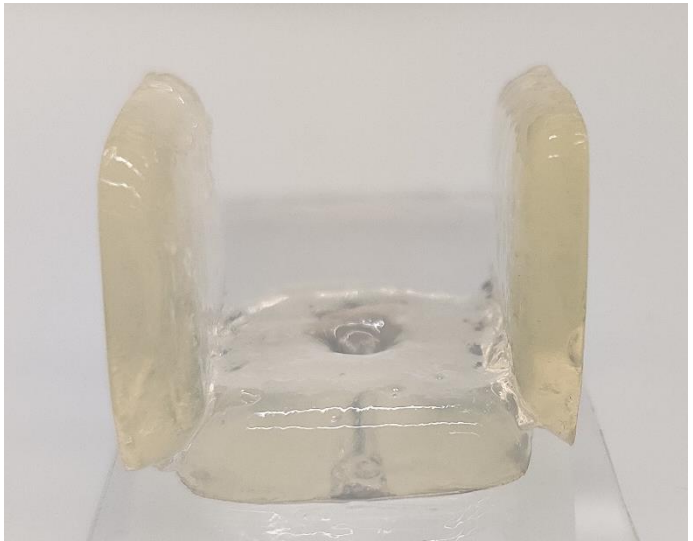
- Heavy equipment: glovebox and 3D bioprinter



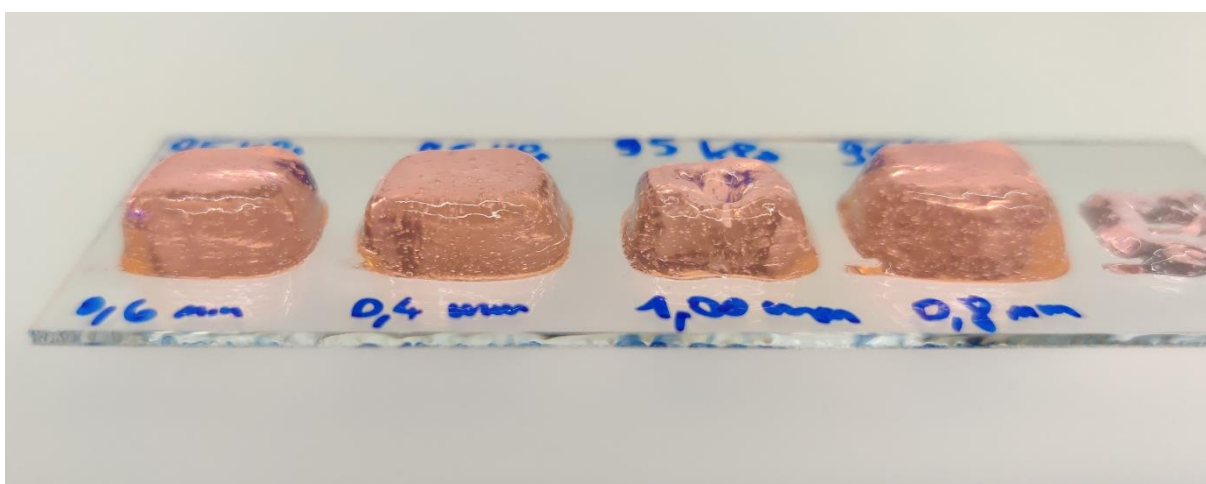
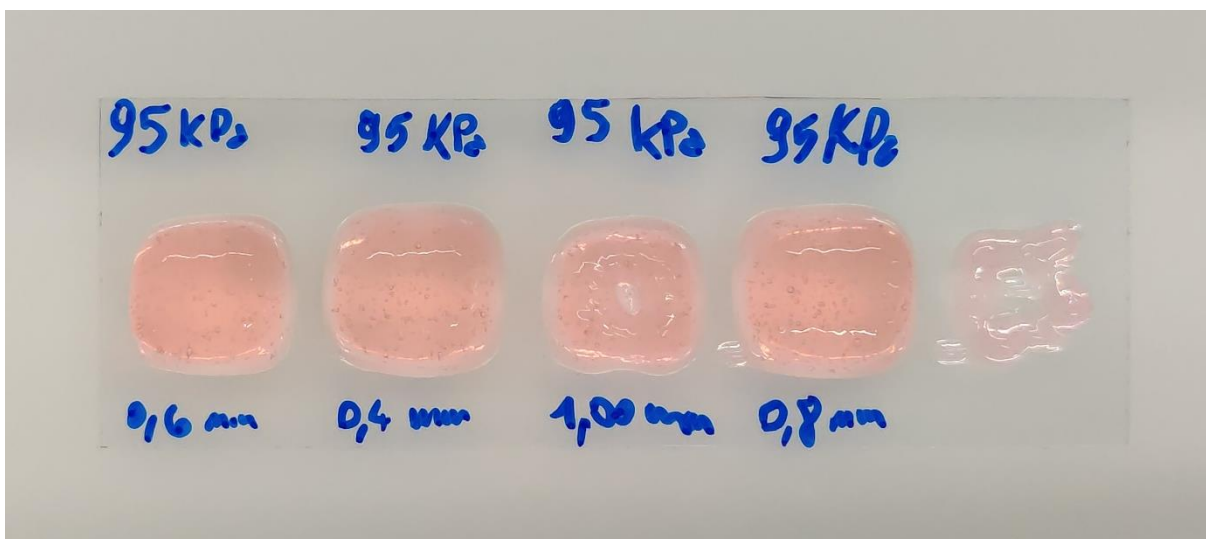
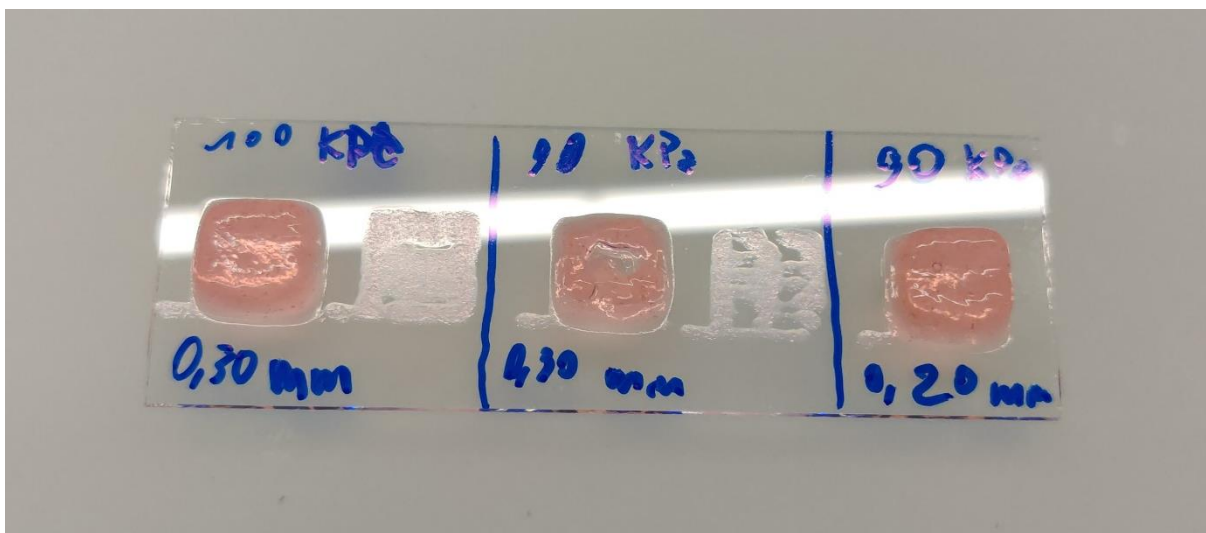
- Special syringes: metal printer tip and bioink, gas and liquid syringes



- Study on adhesive strength of bioink and structural stability



- Study on printing parameters



- **Additional graphs**

